

Strong effects of fast collisions between pulsed optical beams in a linear medium with weak cubic loss

Avner Peleg¹ and Toan T. Huynh²

¹*Department of Mathematics, Azrieli College of Engineering, Jerusalem 9371207, Israel and*

²*Department of Mathematics, University of Medicine and Pharmacy at Ho Chi Minh City, Ho Chi Minh City, Vietnam*

(Dated: October 4, 2022)

Abstract

We investigate fast collisions between pulsed optical beams in a linear medium with weak cubic loss that arises due to nondegenerate two-photon absorption. We introduce a perturbation method with two small parameters and use it to obtain general formulas for the collision-induced changes in the pulsed-beam's shape and amplitude. Moreover, we use the method to design and characterize collision setups that lead to strong localized and nonlocalized intensity reduction effects. The values of the collision-induced changes in the pulsed-beam's shape in both setups are larger by one to two orders of magnitude compared with the values obtained in previous studies of fast two-pulse collisions. Furthermore, we show that for nonlocalized setups, the graph of the collision-induced amplitude shift vs the difference between the first-order dispersion coefficients for the two pulsed-beams has two local minima. This finding represents the first observation of a deviation of the graph from the common funnel shape that was obtained in all previous studies of fast two-pulse collisions in the presence of weak nonlinear loss. The predictions of our perturbation theory are in good agreement with results of numerical simulations with the perturbed linear propagation model, despite the strong collision-induced effects. Our results can be useful for multisequence optical communication links and for reshaping of pulsed optical beams.

Keywords: Pulsed optical beams, two-photon absorption, beam collisions

I. INTRODUCTION

Collisions between optical pulses play an important role in many optical systems. Examples include wavelength-division-multiplexed (WDM) optical communication links [1–5], fiber grating [1, 6, 7], waveguide couplers [1, 8, 9], and Sagnac interferometers [1, 10, 11]. On one hand, the collisions can be beneficially used for optical switching [1, 7, 12–14], pulse compression [12, 15, 16], generation of pulse trains [10], parametric amplification [11], and optical logical gates [17]. On the other hand, the collisions can have harmful effects in WDM communication systems. In these systems, many pulse sequences propagate through the same optical medium. The pulses in each sequence propagate with the same group velocity, but the group velocities are different for pulses from different sequences. As a result, collisions between pulses from different sequences are very frequent, and their cumulative effect can lead to severe transmission degradation and to transmission error [1–5]. For these reasons, many research efforts have been devoted to studying the different effects of collisions between optical pulses [1–5, 12].

In the current work, we study fast collisions between two pulsed optical beams in a linear bulk optical medium with weak cubic loss. We assume that the cubic loss is due to nondegenerate two-photon absorption (2PA), i.e., due to simultaneous absorption of two photons with different wavelengths [18, 19]. Fast two-pulse (or two-beam) collisions are encounters between two optical pulses (or optical beams), in which the interval along which the two pulses overlap (the collision length) is much smaller than all the other length scales in the problem [20]. As described in the preceding paragraph, collisions between optical pulses are very important in WDM communication links. The nonlinearities in these systems are typically weak [2, 21], and almost all collisions are fast [22–24]. Therefore, the study of fast collisions of optical pulses or optical beams in the presence of weak nonlinearities is very relevant to WDM optical communication links. An important problem in this area concerns the characterization of the effects of a single fast two-pulse collision by explicit formulas. Indeed, such characterization enables the evaluation of the cumulative effects of many fast collisions without having to perform a large number of numerical simulations or experiments. Furthermore, it enables the design of methods for compensating the harmful cumulative effects of fast optical pulse collisions.

In Refs. [22, 25], we studied the dynamics of fast two-pulse collisions in linear optical

waveguides with weak cubic loss. We first developed a perturbation method for analyzing the effects of these collisions. We then used the method to show that the expression for the collision-induced amplitude shift in a single collision has the same simple form as the expression for the amplitude shift in a fast collision between two solitons of the cubic nonlinear Schrödinger equation in the presence of weak cubic loss [26]. We also found that within the leading order of the perturbation theory, the shapes of the optical pulses are not changed by the collision. Furthermore, we showed that similar behavior holds in fast collisions between two concentration pulses in the presence of weak quadratic loss in systems described by weakly perturbed diffusion-advection equations [22, 25]. The predictions of our perturbation theory were confirmed by numerical simulations with the perturbed linear propagation equation and the perturbed linear diffusion-advection equation with weak nonlinear loss. The results of Refs. [22, 25] are quite surprising. Indeed, the pulses in weakly perturbed linear optical waveguides are not shape preserving. As a result, the common expectation is that conclusions drawn from analysis of optical soliton collisions would *not* be applicable for collisions between optical pulses in weakly perturbed linear waveguides [2, 12, 15, 27]. However, in Refs. [22, 25], we showed that exactly the opposite is true.

In Ref. [28], we generalized the perturbation method of Refs. [22, 25] to treat fast collisions between two time-independent optical beams in the presence of weak cubic loss in spatial dimension 2. In this case, the collisions are induced by beam-steering, and special techniques are needed to realize and control the steering [29–31]. We used the generalized perturbation approach to show that a fast collision between two time-independent beams leads to a change in the beam shapes in the direction transverse to the vector of relative velocity between the beams. Additionally, we studied the case of a separable initial condition for both beams, which is of special importance, since it describes the electric fields that are produced by many types of lasers [32, 33]. In this case we found that the beam shape in the longitudinal direction is not changed by the collision within the leading order of the perturbative calculation. Furthermore, we showed that for a separable initial condition, the longitudinal part in the expression for the amplitude shift is universal, while the transverse part is not universal and is proportional to the integral of the product of the beam intensities with respect to the transverse coordinate. The predictions of the generalized perturbation theory were confirmed by numerical simulations with the perturbed linear propagation equation with weak cubic loss.

The studies in Refs. [22, 25, 28] were limited to weak collisional effects, that is, the values of the collision-induced amplitude shift and the intensity reduction factor in the collision setups that were considered in these works were small. Although we were able to measure these values in numerical simulations, it is very difficult to measure such small values in experiments. Furthermore, the works in Refs. [22, 25, 28] were limited to spatial dimensions 1 and 2 [34]. As a result, an important property of the collisional effects that exists only in spatial dimension 3, i.e., in collisions between pulsed optical beams, was not addressed in these studies. This property is related to the behavior of the graph of the collision-induced amplitude shift vs the difference between the beam velocities, which is one of the main tools for analyzing the collisional effects. According to the perturbation theory of Refs. [22, 25, 28], this graph has a funnel shape, and does not possess any local extrema. Furthermore, no deviation from the common funnel shape form can exist in the graph for fast collisions in spatial dimensions 1 and 2. This property was verified by numerical simulations in Refs. [22, 25, 28], and was also observed in fast collisions between optical solitons in the presence of weak nonlinear loss [35–38]. Another important aspect of the fast collision problem that was not addressed in previous works concerns the characterization of the differences between the collision-induced effects in localized and nonlocalized collision setups. More specifically, as will be shown in the current paper, the perturbation theory’s formulas for the collision-induced changes in the beam shapes enable the design of localized collision setups, in which the intensity reduction is concentrated mainly near the beam centers, and nonlocalized collision setups, in which the intensity reduction affects the entire main bodies of the beams. The intensity reduction patterns observed in these setups are very different, and these differences can also strongly affect the magnitude of the collision-induced amplitude shift and its dependence on the difference between the beam velocities. Despite the importance of this aspect of the problem, no attempt to characterize the differences between the collisional effects in localized and nonlocalized collision setups was made in previous studies.

In the current paper, we address the important aspects of the fast two-beam collision problem that were overlooked in previous studies. More specifically, we study fast collisions between two pulsed optical beams in a linear optical medium with weak cubic loss in physical setups, in which the collisional effects are relatively strong. The collisions are induced by the difference between the first-order dispersion coefficients for the two pulsed-beams. These

collisions are easier to realize than the collisions between time-independent beams that were studied in Ref. [28], since their experimental realization does not require the application of beam steering. We first introduce a perturbation approach for calculating the effects of a single fast collision between two pulsed-beams. We then use the approach to obtain general explicit expressions for the collision-induced changes in the pulsed-beam's shape and amplitude. Moreover, we use the approach to design and characterize collision setups that lead to strong localized and nonlocalized intensity reduction effects. The values of the collision-induced changes in the pulsed-beam's shape predicted by our perturbation theory are larger by one to two orders of magnitude compared with the values obtained in fast collisions between time-independent beams in Ref. [28] and in fast collisions between optical solitons in spatial dimension 1 in Ref. [39]. The perturbation theory predictions are in good agreement with the results of numerical simulations with the perturbed linear propagation model for both localized and nonlocalized collision setups, despite the relatively strong collision-induced effects.

We gain further insight into the effects of the collisions by studying the dependence of the following two central physical quantities on the difference between the first-order dispersion coefficients for the two pulsed-beams. (1) The final value of the intensity reduction ratio on the propagation axis (the z axis). (2) The collision-induced amplitude shift. The results of the perturbative calculation and numerical simulations for the final value of the intensity reduction ratio on the z axis show that the significant intensity reduction effects are not limited to intermediate differences between the first-order dispersion coefficients, but also exist for large differences. These results hold for both localized and nonlocalized collision setups. Furthermore, the results of the numerical simulations for the nonlocalized collision setups show that the graph of the amplitude shift vs the difference between the first-order dispersion coefficients has two local minima at intermediate values of the difference. These local minima are correctly captured by our perturbative calculation. To our knowledge, this finding represents the first observation of a deviation of the graph of the amplitude shift vs the difference between the first-order dispersion coefficients from the common funnel shape that is obtained in fast collisions between temporal pulses or time-independent beams in linear optical media [22, 25, 28], and in fast collisions between optical solitons [35–38].

We focus our attention on two-beam collisions in the presence of cubic loss, since cubic loss is important in many optical systems [40–43]. Furthermore, cubic loss is the dominant

nonlinear loss mechanism in these systems, and is therefore important in fast optical pulse collisions [22, 25, 28, 35]. The optical medium’s cubic loss is typically due to 2PA [40–43]. Propagation of optical pulses and optical beams in the presence of cubic loss has been studied in many earlier works, both in weakly perturbed linear media [22, 25, 44–47], and in nonlinear media [35, 39, 48–53]. The subject gained further attention in recent years due to the importance of 2PA in silicon nanowaveguides, which are expected to play a key role in many applications in optoelectronic devices [40–42, 54]. In the current paper, we study the effects of weak cubic loss due to nondegenerate 2PA on collisions in a bulk optical medium. We neglect the effects of degenerate 2PA, which arises due to the simultaneous absorption of two photons with the same wavelength. This means that we assume that the effects of cubic loss on single-beam propagation are much weaker compared with the effects of cubic loss on interbeam interaction. This situation can be realized, for example, in certain nonlinear semiconductors, in which degenerate 2PA is much weaker than nondegenerate 2PA [18, 19, 55]. We also assume that the optical medium is weakly nonlinear and neglect the effects of cubic (Kerr) nonlinearity. We point out that this assumption was successfully used in previous experimental and theoretical works, see, e.g., Refs. [44–47]. For similar reasons, we neglect the effects of high-order nonlinear loss on the collisions, and remark that the latter effects can be described by the same perturbation approach that is presented in the current paper (see also Ref. [56], where the calculation was carried out for pulse collisions in spatial dimension 1).

The rest of the paper is organized in the following manner. In Section II, we present our perturbation approach for fast two-beam collisions and its predictions for the collision-induced effects. In Section III, we describe the guiding principles for the design of collision setups that lead to strong localized and nonlocalized intensity reduction. We also present the calculation of the collision-induced changes in the pulsed-beam’s shape and amplitude, and the calculation of the intensity reduction ratio for these setups. In Section IV, we present the results of our numerical simulations with the perturbed linear propagation model, and compare these results with the perturbation theory predictions. We summarize our conclusions in section V.

II. THEORETICAL PREDICTIONS FOR COLLISION-INDUCED EFFECTS

A. Introduction

We consider the dynamics of fast collisions between two pulsed optical beams in a three-dimensional linear optical medium with weak cubic loss, where the cubic loss arises due to nondegenerate 2PA. We assume that the pulsed-beams propagate along the z axis and that the propagation is accurately described by the paraxial approximation [32, 33, 57]. In addition to weak cubic loss, we take into account the effects of first-order and second-order dispersion and isotropic diffraction. Therefore, the dynamics of the fast collision is described by the following weakly perturbed linear propagation model:

$$\begin{aligned} i\partial_{z''}E'_1 + i\tilde{\beta}_{11}\partial_{\tau'}E'_1 - \tilde{\beta}_{21}\partial_{\tau'}^2E'_1/2 + \tilde{d}_{21}\partial_{x'}^2E'_1 + \tilde{d}_{21}\partial_{y'}^2E'_1 &= -2i\rho_3|E'_2|^2E'_1, \\ i\partial_{z''}E'_2 + i\tilde{\beta}_{12}\partial_{\tau'}E'_2 - \tilde{\beta}_{22}\partial_{\tau'}^2E'_2/2 + \tilde{d}_{22}\partial_{x'}^2E'_2 + \tilde{d}_{22}\partial_{y'}^2E'_2 &= -2i\rho_3|E'_1|^2E'_2. \end{aligned} \quad (1)$$

In Eq. (1), E'_j with $j = 1, 2$ are the dimensional electric fields of pulsed-beams 1 and 2, z'' and τ' are the dimensional propagation distance and time, and x' and y' are the dimensional spatial coordinates in the xy plane. In addition, $\tilde{\beta}_{1j}$ and $\tilde{\beta}_{2j}$ are the dimensional first-order and second-order dispersion coefficients, $\tilde{d}_{2j} = \lambda_j/(4\pi)$ are the dimensional diffraction coefficients, where λ_j are the wavelengths, and ρ_3 is the dimensional cubic loss coefficient.

We now make a change of variables of the form

$$z' = z'', \quad \tau = \tau' - \tilde{\beta}_{11}z', \quad E_1(z', x', y', \tau) = E'_1(z'', x', y', \tau'). \quad (2)$$

This means that we go to the retarded reference frame for pulsed-beam 1 (see, e.g., Ref. [12], p. 61). The transformation (2) is important, since it enables the identification of the true small parameters in the fast collision problem, and as a result, the application of the perturbation method and the derivation of explicit approximate formulas for the collision-induced changes in the shapes and amplitudes of the pulsed-beams. Using the transformation (2) in Eq. (1), we obtain:

$$\begin{aligned} i\partial_{z'}E_1 - \tilde{\beta}_{21}\partial_{\tau}^2E_1/2 + \tilde{d}_{21}\partial_{x'}^2E_1 + \tilde{d}_{21}\partial_{y'}^2E_1 &= -2i\rho_3|E_2|^2E_1, \\ i\partial_{z'}E_2 + i\Delta\tilde{\beta}_1\partial_{\tau}E_2 - \tilde{\beta}_{22}\partial_{\tau}^2E_2/2 + \tilde{d}_{22}\partial_{x'}^2E_2 + \tilde{d}_{22}\partial_{y'}^2E_2 &= -2i\rho_3|E_1|^2E_2, \end{aligned} \quad (3)$$

where $\Delta\tilde{\beta}_1 = \tilde{\beta}_{12} - \tilde{\beta}_{11}$.

In order to employ the perturbation theory for the fast collision, we must bring the propagation model to a nondimensional form [58]. For this purpose, we define the dimensionless propagation distance z , the dimensionless time t , the dimensionless spatial coordinates x and y , and the dimensionless electric fields ψ_j by:

$$z = z'/(2L_D), \quad t = \tau/\tau_0, \quad x = x'/x'_0, \quad y = y'/y'_0, \quad \psi_j = E_j/\sqrt{P_0}. \quad (4)$$

In Eq. (4), $L_D = \tau_0^2/|\tilde{\beta}_{21}|$ is the dispersion length, τ_0 is the temporal width of a reference pulsed-beam, x'_0 is the width of a reference pulsed-beam along the x axis, and P_0 is the peak power of the reference pulsed-beam. Using the relations (4) in Eq. (3), we obtain the dimensionless form of the weakly perturbed propagation model:

$$\begin{aligned} i\partial_z\psi_1 - \text{sgn}(\tilde{\beta}_{21})\partial_t^2\psi_1 + d_{21}\partial_x^2\psi_1 + d_{21}\partial_y^2\psi_1 &= -2i\epsilon_3|\psi_2|^2\psi_1, \\ i\partial_z\psi_2 + i\Delta\beta_1\partial_t\psi_2 + \beta_{22}\partial_t^2\psi_2 + d_{22}\partial_x^2\psi_2 + d_{22}\partial_y^2\psi_2 &= -2i\epsilon_3|\psi_1|^2\psi_2. \end{aligned} \quad (5)$$

The coefficients $\Delta\beta_1$ and β_{22} in Eq. (5) are the dimensionless first-order and second-order dispersion coefficients, d_{2j} are the dimensionless diffraction coefficients, and ϵ_3 is the dimensionless cubic loss coefficient. These coefficients are defined by the following relations:

$$\begin{aligned} \Delta\beta_1 &= 2\Delta\tilde{\beta}_1\tau_0/|\tilde{\beta}_{21}|, \quad \beta_{22} = -\tilde{\beta}_{22}/|\tilde{\beta}_{21}|, \quad d_{2j} = \tau_0^2\lambda_j/(2\pi|\tilde{\beta}_{21}|x_0'^2), \\ \epsilon_3 &= 2P_0\tau_0^2\rho_3/|\tilde{\beta}_{21}|. \end{aligned} \quad (6)$$

In the current paper, we study fast collisions in the presence of weak cubic loss. We therefore assume that the coefficients $\Delta\beta_1$ and ϵ_3 satisfy $|\Delta\beta_1| \gg 1$ and $0 < \epsilon_3 \ll 1$.

Our perturbation approach applies for fast collisions between pulsed optical beams with general initial shapes, such that the total energies $\int_{-\infty}^{\infty} dt \int_{-\infty}^{\infty} dx \int_{-\infty}^{\infty} dy |\psi_j(t, x, y, 0)|^2$ are finite. We assume that the initial pulsed-beams can be characterized by the following parameters. (1) The initial amplitudes $A_j(0)$. (2) The initial widths of the pulsed-beams along the t , x , and y axes, $W_{j0}^{(t)}$, $W_{j0}^{(x)}$, and $W_{j0}^{(y)}$. (3) The initial positions of the beam centers (t_{j0}, x_{j0}, y_{j0}) . (4) The initial phases α_{j0} . Thus, the initial electric fields can be written as:

$$\psi_j(t, x, y, 0) = A_j(0)h_j(t, x, y) \exp(i\alpha_{j0}), \quad (7)$$

where $h_j(t, x, y)$ is a real-valued function that characterizes the initial spatio-temporal distribution of the electric field. We are equally interested in the important case, where the

initial electric fields of the two pulsed-beams are separable, i.e., where each of the functions $\psi_j(t, x, y, 0)$ is a product of three functions of t , x , and y :

$$\begin{aligned} \psi_j(t, x, y, 0) &= A_j(0)h_j^{(t)}[(t - t_{j0})/W_{j0}^{(t)}]h_j^{(x)}[(x - x_{j0})/W_{j0}^{(x)}] \\ &\times h_j^{(y)}[(y - y_{j0})/W_{j0}^{(y)}] \exp(i\alpha_{j0}). \end{aligned} \quad (8)$$

This initial condition is of special importance since it describes the electric fields that are produced by many lasers [32, 33].

In the current paper, we demonstrate strong collision-induced effects in complete fast collisions. We therefore obtain conditions on the physical parameter values for these collisions. The complete collision assumption means that the pulsed-beams are well-separated before and after the collision. As a result, in these collisions, the values of the t coordinate of the pulsed-beam centers at $z = 0$ and at the final propagation distance z_f , t_{j0} and $t_j(z_f)$, must satisfy $|t_{20} - t_{10}| \gg W_{10}^{(t)} + W_{20}^{(t)}$ and $|t_2(z_f) - t_1(z_f)| \gg W_1^{(t)}(z_f) + W_2^{(t)}(z_f)$, where $W_j^{(t)}(z_f)$ are the pulsed-beam widths along the t axis at $z = z_f$. To obtain the condition for a fast collision, we define the collision length Δz_c as the distance along which the temporal widths of the pulsed-beams overlap. From this definition it follows that $\Delta z_c = 2(W_{10}^{(t)} + W_{20}^{(t)})/|\Delta\beta_1|$. The fast collision assumption means that Δz_c is much smaller than the length scale $z_D^{(min)}$, which is the smallest dispersion length or diffraction length in the problem. By definition, $z_D^{(min)} = \min \left\{ z_{d1}^{(t)}, z_{d2}^{(t)}, z_{D1}^{(x)}, z_{D2}^{(x)}, z_{D1}^{(y)}, z_{D2}^{(y)} \right\}$, where $z_{dj}^{(t)}$ are the dispersion lengths of the pulsed-beams, and $z_{Dj}^{(x)}$ and $z_{Dj}^{(y)}$ are the diffraction lengths along the x and y axes. Requiring that $\Delta z_c \ll z_D^{(min)}$, we obtain $2(W_{10}^{(t)} + W_{20}^{(t)}) \ll |\Delta\beta_1|z_D^{(min)}$, as the condition for a fast collision.

B. The perturbation approach and its predictions for a general initial condition

We present here a relatively brief description of the perturbative calculation of the collision-induced changes in the shapes and amplitudes of the pulsed-beams for the general initial condition (7). The results for the separable initial condition (8) are presented in section II C. The current treatment is a generalization of the calculation that was carried out in Ref. [28] for fast collisions between time-independent optical beams (in the absence of dispersion effects). Since the main steps in the current perturbative calculation are similar to the ones described in Ref. [28] for the time-independent case, we concentrate here only on

those steps and results, which are essential for the understanding of the material in sections III and IV. We refer the reader, who is interested in more details, to the description of the time-independent version of the approach in Ref. [28].

In the first step in the perturbative calculation, we look for a solution of Eq. (5) in the form:

$$\psi_j(t, x, y, z) = \psi_{j0}(t, x, y, z) + \phi_j(t, x, y, z), \quad (9)$$

where $j = 1, 2$, ψ_{j0} are the solutions of the unperturbed linear propagation equations, and ϕ_j describe corrections to the ψ_{j0} due to the effects of cubic loss on the collision. By definition, the ψ_{j0} satisfy the equations

$$i\partial_z\psi_{10} - \text{sgn}(\tilde{\beta}_{21})\partial_t^2\psi_{10} + d_{21}\partial_x^2\psi_{10} + d_{21}\partial_y^2\psi_{10} = 0, \quad (10)$$

and

$$i\partial_z\psi_{20} + i\Delta\beta_1\partial_t\psi_{20} + \beta_{22}\partial_t^2\psi_{20} + d_{22}\partial_x^2\psi_{20} + d_{22}\partial_y^2\psi_{20} = 0. \quad (11)$$

We expand the ϕ_j in perturbation series with respect to the two small parameters ϵ_3 and $1/|\Delta\beta_1|$. We are interested in the first nonzero term in each of these expansions. These first nonzero terms in the expansions represent the leading-order collision-induced changes in the pulse shapes, and we therefore refer to them as the leading-order expressions for the ϕ_j .

We substitute the relation (9) into Eq. (5) and use Eqs. (10) and (11) to obtain equations for the dynamics of the ϕ_j . We concentrate on the calculation of ϕ_1 , since the calculation of ϕ_2 is similar. To obtain the equation for the leading-order expression for ϕ_1 we must neglect high-order terms containing products of ϵ_3 with ϕ_1 or ϕ_2 in the equation obtained after the substitution. Thus, the substitution and the subsequent approximations yield the following equation for the leading-order expression for ϕ_1 :

$$i\partial_z\phi_1 - \text{sgn}(\tilde{\beta}_{21})\partial_t^2\phi_1 + d_{21}\partial_x^2\phi_1 + d_{21}\partial_y^2\phi_1 = -2i\epsilon_3|\psi_{20}|^2\psi_{10}. \quad (12)$$

Note that for brevity and simplicity of notation, in Eq. (12), we denote the leading-order expression for ϕ_1 by ϕ_1 . This notation is also used in the remainder of the paper.

In solving the equation for ϕ_1 , we recognize two different intervals along the z axis, the collision interval and the post-collision interval. To define these intervals, we introduce the collision distance z_c , which is the distance at which the t coordinates of the pulsed-beam

centers coincide, i.e., $t_1(z_c) = t_2(z_c)$. The collision interval is the small interval $z_c - \Delta z_c/2 \leq z \leq z_c + \Delta z_c/2$ around z_c , in which the two pulsed-beams overlap. This interval is an effective boundary layer in our perturbative calculation. The post-collision interval is the interval $z > z_c + \Delta z_c/2$, in which the pulsed-beams no longer overlap.

1. *Calculation of the collision-induced effects in the collision interval*

We substitute $\psi_{j0}(t, x, y, z) = A_j(z)\Psi_{j0}(t, x, y, z) \exp[i\chi_{j0}(t, x, y, z)]$ and $\phi_1(t, x, y, z) = \Phi_1(t, x, y, z) \exp[i\chi_{10}(t, x, y, z)]$ into Eq. (12), where $A_j(z)$ are the z -dependent amplitudes of the pulsed-beams, and Ψ_{j0} and χ_{j0} are real-valued. This substitution yields an equation for Φ_1 (see also Ref. [28] for the time-independent case). Neglecting the high-order terms in the latter equation, we arrive at the following equation for Φ_1 in the leading order of the perturbative calculation:

$$\partial_z \Phi_1 = -2\epsilon_3 A_1(z) A_2^2(z) \Psi_{20}^2 \Psi_{10}. \quad (13)$$

As we will see, the simple form of the equation for the dynamics of Φ_1 in the collision interval is important in enabling the design of collision setups that lead to strong intensity reduction effects.

We calculate the collision-induced amplitude shift of pulsed-beam 1 from the net change in Φ_1 in the collision interval, $\Delta\Phi_1(t, x, y, z_c) = \Phi_1(t, x, y, z_c + \Delta z_c/2) - \Phi_1(t, x, y, z_c - \Delta z_c/2)$. $\Delta\Phi_1(t, x, y, z_c)$ is calculated by integration of Eq. (13) with respect to z over the collision interval:

$$\Delta\Phi_1(t, x, y, z_c) = -2\epsilon_3 \int_{z_c - \Delta z_c/2}^{z_c + \Delta z_c/2} dz' A_1(z') A_2^2(z') \Psi_{10}(t, x, y, z') \Psi_{20}^2(t, x, y, z'). \quad (14)$$

We notice that Ψ_{20} is the only function in the integrand on the right hand side of Eq. (14) that contains fast variations in z , which are of order 1. Therefore, we can approximate $A_j(z)$ and $\Psi_{10}(t, x, y, z)$ by $A_j(z_c^-)$ and $\Psi_{10}(t, x, y, z_c)$, where $A_j(z_c^-)$ is the limit from the left of $A_j(z)$ at z_c . Additionally, since outside of the collision interval loss is negligible, we can set $A_j(z_c^-) = A_j(0)$. Furthermore, in calculating the integral, we can take into account in an exact manner only the fast dependence of Ψ_{20} on z , which is contained in the factors $\tilde{t} = t - t_{20} - \Delta\beta_1 z$, and replace z by z_c everywhere else in the expression for Ψ_{20} . This approximation of $\Psi_{20}(t, x, y, z)$ is denoted by $\bar{\Psi}_{20}(\tilde{t}, x, y, z_c)$. In addition, we assume

that the approximate integrand $\bar{\Psi}_{20}^2(\tilde{t}, x, y, z_c)$ is sharply peaked in a small interval around z_c . As a result, we can extend the integral's limits to $-\infty$ and ∞ (see also Ref. [28]). Carrying out all these approximations and also changing the integration variable from z' to $\tilde{t} = t - t_{20} - \Delta\beta_1 z'$, we obtain:

$$\Delta\Phi_1(t, x, y, z_c) = -\frac{2\epsilon_3 A_1(0) A_2^2(0)}{|\Delta\beta_1|} \Psi_{10}(t, x, y, z_c) \int_{-\infty}^{\infty} d\tilde{t} \bar{\Psi}_{20}^2(\tilde{t}, x, y, z_c). \quad (15)$$

From Eq. (15) it follows that inside the collision interval, the temporal shape of the pulsed-beam is preserved, while the spatial shape is changed by the collision. It also follows that one can use the collision to induce strong localized changes in the spatial shape of one of the pulsed-beams (e.g., pulsed-beam 1) by choosing a second pulsed-beam that is spatially localized around the z axis at $z = z_c$. In the current paper, we use these properties of the fast collision to design collision setups that lead to relatively strong changes in the spatial shapes of the pulsed-beams even for small values of ϵ_3 and $1/|\Delta\beta_1|$.

The collision-induced change in the shape of pulsed-beam 1 in the collision interval $\Delta\Phi_1(t, x, y, z_c)$ is related to the collision-induced amplitude shift $\Delta A_1^{(c)}$ by:

$$\Delta A_1^{(c)} = C_{p1}^{-1} \int_{-\infty}^{\infty} dt \int_{-\infty}^{\infty} dx \int_{-\infty}^{\infty} dy \Psi_{10}(t, x, y, z_c) \Delta\Phi_1(t, x, y, z_c), \quad (16)$$

where

$$C_{p1} = \int_{-\infty}^{\infty} dt \int_{-\infty}^{\infty} dx \int_{-\infty}^{\infty} dy \Psi_{10}^2(t, x, y, 0). \quad (17)$$

Substitution of Eq. (15) into Eq. (16) yields the following equation for the collision-induced amplitude shift of pulsed-beam 1 for the general initial condition (7):

$$\Delta A_1^{(c)} = -\frac{2\epsilon_3 A_1(0) A_2^2(0)}{C_{p1} |\Delta\beta_1|} \int_{-\infty}^{\infty} dt \int_{-\infty}^{\infty} dx \int_{-\infty}^{\infty} dy \Psi_{10}^2(t, x, y, z_c) \int_{-\infty}^{\infty} d\tilde{t} \bar{\Psi}_{20}^2(\tilde{t}, x, y, z_c). \quad (18)$$

Note that Eq. (18) for $\Delta A_1^{(c)}$ contains integrals with respect to x and y , while Eq. (15) for $\Delta\Phi_1(t, x, y, z_c)$ does not. As a result, it is possible to find collision setups, which lead to strong localized changes in the spatial shape of one of the pulsed-beams (e.g., pulsed-beam 1), and for which the collision-induced amplitude shift is relatively small.

2. Calculation of $\phi_1(t, x, y, z)$ in the post-collision interval

In the post-collision interval, $z > z_c + \Delta z_c/2$, the pulsed-beams are no longer overlapping. Consequently, the nonlinear interaction terms $-2i\epsilon_3 |\psi_2|^2 \psi_1$ and $-2i\epsilon_3 |\psi_1|^2 \psi_2$ are negligible

in this interval. Therefore, in the leading order of the perturbation theory, the equation for ϕ_1 in the post-collision interval is the unperturbed linear propagation equation

$$i\partial_z\phi_1 - \text{sgn}(\tilde{\beta}_{21})\partial_t^2\phi_1 + d_{21}\partial_x^2\phi_1 + d_{21}\partial_y^2\phi_1 = 0. \quad (19)$$

In a fast collision $|\Delta\beta_1| \gg 1$, and as a result, $\Delta\Phi_1(t, x, y, z_c) \simeq \Phi_1(t, x, y, z_c^+)$, where $\Phi_1(t, x, y, z_c^+)$ is the limit from the right of $\Phi_1(t, x, y, z)$ at $z = z_c$. It follows that the initial condition for Eq. (19) is:

$$\phi_1(t, x, y, z_c^+) = \Phi_1(t, x, y, z_c^+) \exp[i\chi_{10}(t, x, y, z_c)], \quad (20)$$

where $\Phi_1(t, x, y, z_c^+)$ is given by Eq. (15). The solution of Eq. (19) with the initial condition (20) is

$$\phi_1(t, x, y, z) = \mathcal{F}^{-1} \left(\hat{\phi}_1(\omega, k_1, k_2, z_c^+) \exp\{i[\text{sgn}(\tilde{\beta}_{21})\omega^2 - d_{21}k_1^2 - d_{21}k_2^2](z - z_c)\} \right), \quad (21)$$

where $\hat{\phi}_1(\omega, k_1, k_2, z_c^+) = \mathcal{F}(\phi_1(t, x, y, z_c^+))$, and \mathcal{F} and \mathcal{F}^{-1} denote the Fourier transform and the inverse Fourier transform with respect to t, x , and y . We can write $\phi_1(t, x, y, z)$ in the form $\phi_1(t, x, y, z) = |\phi_1(t, x, y, z)| \exp[i\chi_1^{(tot)}(t, x, y, z)]$, where $\chi_1^{(tot)}(t, x, y, z)$ is a real-valued phase factor. In general, $\chi_1^{(tot)}(t, x, y, z) \neq \chi_{10}(t, x, y, z)$ inside the post-collision interval. We therefore define the difference between the phase factors of ψ_{10} and ϕ_1 by:

$$\Delta\chi_1^{(tot)}(t, x, y, z) = \chi_{10}(t, x, y, z) - \chi_1^{(tot)}(t, x, y, z). \quad (22)$$

C. The predictions of the perturbation approach for a separable initial condition

Let us briefly describe the perturbation theory predictions for the collision-induced effects in the important case, where the initial condition is given by Eq. (8), which is separable for both pulsed-beams. This case is of special interest for two reasons. First, this initial condition corresponds to the output electric field from many types of lasers [32, 33]. Second, in this case, it is possible to simplify the expressions for the collision-induced changes in the shape and amplitude of the pulsed-beams even further, and by this, obtain deeper insight into the collision dynamics. For brevity, we present here only the end results of the calculations for $\Delta\Phi_1(t, x, y, z_c)$, $\Delta A_1^{(c)}$, and $\phi_1(t, x, y, z)$. We refer the interested reader to Ref. [28] for the details of the derivations that were carried out for time-independent beams.

We first note that the solutions ψ_{j0} of the unperturbed linear propagation equations (10) and (11) with the separable initial condition (8) and with unit amplitude can be written as:

$$\psi_{j0}(t, x, y, z) = g_j^{(t)}(t, z)g_j^{(x)}(x, z)g_j^{(y)}(y, z) \exp(i\alpha_{j0}), \quad (23)$$

where

$$\begin{aligned} g_j^{(t)}(t, z) &= G_j^{(t)}(t, z) \exp \left[i\chi_{j0}^{(t)}(t, z) \right], \quad g_j^{(x)}(x, z) = G_j^{(x)}(x, z) \exp \left[i\chi_{j0}^{(x)}(x, z) \right], \\ g_j^{(y)}(y, z) &= G_j^{(y)}(y, z) \exp \left[i\chi_{j0}^{(y)}(y, z) \right], \end{aligned} \quad (24)$$

and $G_j^{(t)}(t, z)$, $G_j^{(x)}(x, z)$, $G_j^{(y)}(y, z)$, $\chi_{j0}^{(t)}(t, z)$, $\chi_{j0}^{(x)}(x, z)$, and $\chi_{j0}^{(y)}(y, z)$ are real-valued. These solutions can also be expressed in the form

$$\psi_{j0}(t, x, y, z) = \Psi_{j0}(t, x, y, z) \exp [i\chi_{j0}(t, x, y, z)], \quad (25)$$

where $\Psi_{j0}(t, x, y, z) = G_j^{(t)}(t, z)G_j^{(x)}(x, z)G_j^{(y)}(y, z)$, and

$$\chi_{j0}(t, x, y, z) = \chi_{j0}^{(t)}(t, z) + \chi_{j0}^{(x)}(x, z) + \chi_{j0}^{(y)}(y, z) + \alpha_{j0} \quad (26)$$

is the overall phase factor.

For a separable initial condition, one can use the conservation of the total energy for the unperturbed linear propagation equation to further simplify the expressions for the collision-induced changes in the pulsed-beam's amplitude and shape. Using this conservation law together with Eq. (8), we find

$$\int_{-\infty}^{\infty} dt G_j^{(t)2}(t, z) = \int_{-\infty}^{\infty} dt G_j^{(t)2}(t, 0) = W_{j0}^{(t)} \int_{-\infty}^{\infty} ds h_j^{(t)2}(s) = W_{j0}^{(t)} c_{pj}^{(t)}, \quad (27)$$

$$\int_{-\infty}^{\infty} dx G_j^{(x)2}(x, z) = \int_{-\infty}^{\infty} dx G_j^{(x)2}(x, 0) = W_{j0}^{(x)} \int_{-\infty}^{\infty} ds h_j^{(x)2}(s) = W_{j0}^{(x)} c_{pj}^{(x)}, \quad (28)$$

and

$$\int_{-\infty}^{\infty} dy G_j^{(y)2}(y, z) = \int_{-\infty}^{\infty} dy G_j^{(y)2}(y, 0) = W_{j0}^{(y)} \int_{-\infty}^{\infty} ds h_j^{(y)2}(s) = W_{j0}^{(y)} c_{pj}^{(y)}. \quad (29)$$

Equations (27)-(29) define the constants $c_{pj}^{(t)}$, $c_{pj}^{(x)}$, and $c_{pj}^{(y)}$, which appear in the expressions for $\Delta A_1^{(e)}$, $\Delta \Phi_1$, and ϕ_1 .

1. *Collision-induced effects in the collision interval*

In the case of a separable initial condition, one can simplify Eq. (15) for the collision-induced change in the shape of pulsed-beam 1 in the collision interval to the following form:

$$\begin{aligned} \Delta\Phi_1(t, x, y, z_c) = & -\frac{2\epsilon_3 A_1(0) A_2^2(0)}{|\Delta\beta_1|} c_{p2}^{(t)} W_{20}^{(t)} \\ & \times G_1^{(t)}(t, z_c) G_1^{(x)}(x, z_c) G_1^{(y)}(y, z_c) G_2^{(x)2}(x, z_c) G_2^{(y)2}(y, z_c). \end{aligned} \quad (30)$$

From Eq. (30) it follows that when the initial condition is separable, the shape of the pulsed-beam does not change at all due to the collision (see also subsection II C 2). Moreover, as will be demonstrated in section III, the simple form of Eq. (30) can be exploited for designing collision setups that lead to localized and nonlocalized strong intensity reduction effects.

The collision-induced amplitude shift for pulsed-beam 1 in the case of a separable initial condition is given by:

$$\begin{aligned} \Delta A_1^{(c)} = & -\frac{2\epsilon_3 A_1(0) A_2^2(0)}{|\Delta\beta_1|} \frac{c_{p2}^{(t)} W_{20}^{(t)}}{c_{p1}^{(x)} W_{10}^{(x)} c_{p1}^{(y)} W_{10}^{(y)}} \\ & \times \int_{-\infty}^{\infty} dx G_1^{(x)2}(x, z_c) G_2^{(x)2}(x, z_c) \int_{-\infty}^{\infty} dy G_1^{(y)2}(y, z_c) G_2^{(y)2}(y, z_c). \end{aligned} \quad (31)$$

We observe that Eq. (31) has the form

$$\Delta A_1^{(c)} = -(\text{overall factor}) \times (\text{temporal factor}) \times (\text{spatial factor}), \quad (32)$$

where the overall factor is $2\epsilon_3 A_1(0) A_2^2(0)/|\Delta\beta_1|$, and the temporal factor is $c_{p2}^{(t)} W_{20}^{(t)}$. Furthermore, the temporal factor is universal in the sense that it does not depend on the exact details of the initial pulsed-beam shapes and on the collision distance z_c .

2. *Calculation of $\phi_1(t, x, y, z)$ in the post-collision interval*

We now turn to describe the calculation of $\phi_1(t, x, y, z)$ in the post-collision interval for a separable initial condition. The dynamics of $\phi_1(t, x, y, z)$ is still described by Eq. (19). The initial condition for Eq. (19) can now be written as

$$\phi_1(t, x, y, z_c^+) = -\tilde{a}_1 g_1^{(t)}(t, z_c) g_{12}^{(x)}(x, z_c) g_{12}^{(y)}(y, z_c) \exp(i\alpha_{10}), \quad (33)$$

where

$$\tilde{a}_1 = 2\epsilon_3 A_1(0) A_2^2(0) c_{p2}^{(t)} W_{20}^{(t)} / |\Delta\beta_1|, \quad (34)$$

and

$$g_{12}^{(x)}(x, z_c) = g_1^{(x)}(x, z_c)G_2^{(x)2}(x, z_c), \quad g_{12}^{(y)}(y, z_c) = g_1^{(y)}(y, z_c)G_2^{(y)2}(y, z_c). \quad (35)$$

It is then possible to show that the expression for $\phi_1(t, x, y, z)$ in the post-collision interval is

$$\begin{aligned} \phi_1(t, x, y, z) = & -\tilde{a}_1 g_1^{(t)}(t, z) \mathcal{F}^{-1} \left(\hat{g}_{12}^{(x)}(k_1, z_c) \exp[-id_{21}k_1^2(z - z_c)] \right) \\ & \times \mathcal{F}^{-1} \left(\hat{g}_{12}^{(y)}(k_2, z_c) \exp[-id_{21}k_2^2(z - z_c)] \right) \exp(i\alpha_{10}), \end{aligned} \quad (36)$$

where $\hat{g}_{12}^{(x)}(k_1, z_c)$ and $\hat{g}_{12}^{(y)}(k_2, z_c)$ are the Fourier transforms of $g_{12}^{(x)}(x, z)$ and $g_{12}^{(y)}(y, z)$ with respect to x and y , respectively. We observe that when the initial condition is separable for both pulsed-beams the t dependences of $\phi_1(t, x, y, z)$ and $\psi_{10}(t, x, y, z)$ are identical for $z > z_c$. It follows that in this case, the temporal shape of the pulsed-beam is not changed by the collision at all. In contrast, the spatial shape of the pulsed-beam is changed by the collision, and this change is proportional to the product of the two inverse Fourier transforms on the right hand side of Eq. (36).

The real-valued phase factor $\chi_1^{(tot)}(t, x, y, z)$ associated with $\phi_1(t, x, y, z)$ can be written as

$$\chi_1^{(tot)}(t, x, y, z) = \chi_{10}^{(t)}(t, z) + \chi_1^{(x)}(x, z) + \chi_1^{(y)}(y, z) + \alpha_{10} + \pi, \quad (37)$$

where $\chi_1^{(x)}(x, z)$ and $\chi_1^{(y)}(y, z)$ are the phase factors associated with $\mathcal{F}^{-1} \left(\hat{g}_{12}^{(x)}(k_1, z_c) \exp[-id_{21}k_1^2(z - z_c)] \right)$ and $\mathcal{F}^{-1} \left(\hat{g}_{12}^{(y)}(k_2, z_c) \exp[-id_{21}k_2^2(z - z_c)] \right)$, respectively. Using Eqs. (26) and (37) we obtain that in the case of a separable initial condition, the phase factor difference $\Delta\chi_1^{(tot)}$ between ψ_{10} and ϕ_1 is given by:

$$\Delta\chi_1^{(tot)}(t, x, y, z) = \chi_{10}^{(x)}(x, z) + \chi_{10}^{(y)}(y, z) - \chi_1^{(x)}(x, z) - \chi_1^{(y)}(y, z) - \pi. \quad (38)$$

III. COLLISION SETUPS THAT LEAD TO STRONG INTENSITY REDUCTION EFFECTS

In this section, we describe the guiding principles for design of collision setups that lead to strong localized and nonlocalized intensity reduction effects. We also present the calculation of the collision-induced change in the pulsed-beam's shape and amplitude, and the calculation of the intensity reduction factor for these setups.

A. Calculation of $\phi_1(t, x, y, z)$ and $\Delta A_1^{(c)}$ for Gaussian pulsed-beams

We consider a separable initial condition in the form of two Gaussian pulsed-beams:

$$\begin{aligned}\psi_1(t, x, y, 0) &= A_1(0) \exp \left[-\frac{t^2}{2W_{10}^{(t)2}} - \frac{x^2}{2W_{10}^{(x)2}} - \frac{y^2}{2W_{10}^{(y)2}} + i\alpha_{10} \right], \\ \psi_2(t, x, y, 0) &= A_2(0) \exp \left[-\frac{(t - t_{20})^2}{2W_{20}^{(t)2}} - \frac{x^2}{2W_{20}^{(x)2}} - \frac{y^2}{2W_{20}^{(y)2}} + i\alpha_{20} \right].\end{aligned}\quad (39)$$

We consider this form of the initial pulsed-beam shapes, since it is highly accessible for laser-beam propagation experiments [32, 33]. In addition, this choice allows us to obtain an explicit formula for ϕ_1 in the post-collision interval. We point out that Eq. (36) of our perturbation approach can be used for calculating ϕ_1 for general separable pulsed-beam shapes of the form (8). However, the latter calculation would require numerical integration of the integrals appearing on the right hand side of Eq. (36).

Since the initial condition is separable, we can calculate ϕ_1 by employing Eq. (36). Using Eq. (27), we find $c_{p2}^{(t)} = \pi^{1/2}$ and

$$\tilde{a}_1 = 2\pi^{1/2}\epsilon_3 A_1(0)A_2^2(0)W_{20}^{(t)}/|\Delta\beta_1|. \quad (40)$$

The solution of the unperturbed linear propagation equation with the initial condition (39) yields the following expression for $g_1^{(t)}(t, z)$:

$$g_1^{(t)}(t, z) = \frac{W_{10}^{(t)}}{(W_{10}^{(t)4} + 4z^2)^{1/4}} \exp \left[-\frac{W_{10}^{(t)2}t^2}{2(W_{10}^{(t)4} + 4z^2)} + i\chi_{10}^{(t)}(t, z) \right], \quad (41)$$

where

$$\chi_{10}^{(t)}(t, z) = \frac{1}{2}\text{sgn}(\tilde{\beta}_{21}) \arctan \left(\frac{2z}{W_{10}^{(t)2}} \right) - \frac{\text{sgn}(\tilde{\beta}_{21})t^2z}{W_{10}^{(t)4} + 4z^2}. \quad (42)$$

The two inverse Fourier transforms on the right hand side of Eq. (36) are calculated in Appendix A. The two calculations are similar to one another. Furthermore, the results can be expressed in a single formula that has the following form:

$$\begin{aligned}\mathcal{F}^{-1} \left(\hat{g}_{12}^{(u)}(k_u, z_c) \exp[-id_{21}k_u^2(z - z_c)] \right) &= \\ &= \frac{W_{10}^{(u)}W_{20}^{(u)2} \exp \left[-q_1^{(u)}(z_c)u^2/R_1^{(u)4}(z, z_c) + i\chi_{11}^{(u)}(u, z) \right]}{(W_{10}^{(u)4} + 4d_{21}^2z_c^2)^{1/4}(W_{20}^{(u)4} + 4d_{22}^2z_c^2)^{1/2}R_1^{(u)}(z, z_c)},\end{aligned}\quad (43)$$

where the u stands for 1 or 2 in k_u , and for x or y , respectively, everywhere else in the formula. The quantities $q_1^{(u)}(z_c)$, $R_1^{(u)}(z, z_c)$, and $\chi_1^{(u)}(u, z)$ in Eq. (43) are given by Eqs. (A3), (A8), and (A9) in Appendix A. Substitution of Eqs. (40)-(43) into Eq. (36) yields the following expression for $\phi_1(t, x, y, z)$:

$$\begin{aligned} \phi_1(t, x, y, z) &= \frac{\tilde{a}_1 W_{10}^{(t)} W_{10}^{(x)} W_{10}^{(y)} W_{20}^{(x)2} W_{20}^{(y)2}}{(W_{10}^{(t)4} + 4z^2)^{1/4} (W_{10}^{(x)4} + 4d_{21}^2 z_c^2)^{1/4} (W_{10}^{(y)4} + 4d_{21}^2 z_c^2)^{1/4}} \\ &\times \left[(W_{20}^{(x)4} + 4d_{22}^2 z_c^2)^{1/2} (W_{20}^{(y)4} + 4d_{22}^2 z_c^2)^{1/2} R_1^{(x)}(z, z_c) R_1^{(y)}(z, z_c) \right]^{-1} \\ &\times \exp \left[-\frac{W_{10}^{(t)2} t^2}{2(W_{10}^{(t)4} + 4z^2)} - \frac{q_1^{(x)}(z_c) x^2}{R_1^{(x)4}(z, z_c)} - \frac{q_1^{(y)}(z_c) y^2}{R_1^{(y)4}(z, z_c)} + i\chi_1^{(tot)}(t, x, y, z) \right], \end{aligned} \quad (44)$$

where the total phase factor $\chi_1^{(tot)}$ is of the form (37), $\chi_{10}^{(t)}$ is given by Eq. (42), and $\chi_1^{(x)}$ and $\chi_1^{(y)}$ are given by Eq. (A9) in Appendix A. We observe that the expression for ϕ_1 is rather complicated even for the relatively simple Gaussian initial condition (39). For this reason, Eq. (44) will not be directly used in the design of the collision setups that lead to significant intensity reduction effects. Instead, we will use an expression that is based on the much simpler form of Eq. (30) for the collision-induced change in the pulsed-beam's shape in the collision-interval.

The equation for the collision-induced amplitude shift $\Delta A_1^{(c)}$ is obtained by employing Eq. (31). Using the expressions for the solutions of the unperturbed linear propagation equation with the initial condition (39) in Eq. (31), we find:

$$\begin{aligned} \Delta A_1^{(c)} &= \frac{-2\pi^{1/2} \epsilon_3 A_1(0) A_2^2(0)}{|\Delta\beta_1|} W_{10}^{(x)} W_{10}^{(y)} W_{20}^{(t)} W_{20}^{(x)2} W_{20}^{(y)2} \\ &\times \left[W_{10}^{(x)2} (W_{20}^{(x)4} + 4d_{22}^2 z_c^2) + W_{20}^{(x)2} (W_{10}^{(x)4} + 4d_{21}^2 z_c^2) \right]^{-1/2} \\ &\times \left[W_{10}^{(y)2} (W_{20}^{(y)4} + 4d_{22}^2 z_c^2) + W_{20}^{(y)2} (W_{10}^{(y)4} + 4d_{21}^2 z_c^2) \right]^{-1/2}. \end{aligned} \quad (45)$$

B. The fractional intensity reduction factor

The main physical quantity, which is used for estimating the strength of the collisional effects, is the fractional intensity reduction factor. We therefore discuss here the definition and the basic properties of this quantity. The fractional intensity reduction factor for pulsed-beam 1 $\Delta I_1^{(r)}$ is defined by:

$$\Delta I_1^{(r)}(t, x, y, z) = \frac{\tilde{I}_1(t, x, y, z) - I_1(t, x, y, z)}{\tilde{I}_1(t, x, y, z)} = 1 - \frac{I_1(t, x, y, z)}{A_1^2(0) \Psi_{10}^2(t, x, y, z)}, \quad (46)$$

where $I_1(t, x, y, z) = |\psi_1(t, x, y, z)|^2$ is the intensity of pulsed-beam 1 in the presence of cubic loss, and $\tilde{I}_1(t, x, y, z) = A_1^2(0)\Psi_{10}^2(t, x, y, z)$ is the intensity of pulsed-beam 1 in the absence of cubic loss. It follows that $\Delta I_1^{(r)}$ measures the ratio between the intensity decrease of pulsed-beam 1, which is caused by the effects of cubic loss on the collision, and the intensity of the pulsed-beam for unperturbed single-beam propagation.

The approximate prediction of the perturbation theory for the fractional intensity reduction factor, which we denote by $\Delta I_1^{(r)(1)}$, is obtained by substituting Eq. (9) into Eq. (46) and by expanding the result up to order $\epsilon_3/|\Delta\beta_1|$. This calculation yields:

$$\Delta I_1^{(r)(1)}(t, x, y, z) = -\frac{\psi_{10}(t, x, y, z)\phi_1^*(t, x, y, z) + \psi_{10}^*(t, x, y, z)\phi_1(t, x, y, z)}{A_1(0)\Psi_{10}^2(t, x, y, z)}. \quad (47)$$

Using the relations $\psi_{10} = \Psi_{10} \exp[i\chi_{10}]$ and $\phi_1 = |\phi_1| \exp[i\chi_1^{(tot)}]$, we obtain:

$$\Delta I_1^{(r)(1)}(t, x, y, z) = -\frac{2|\phi_1(t, x, y, z)| \cos \left[\Delta\chi_1^{(tot)}(t, x, y, z) \right]}{A_1(0)\Psi_{10}(t, x, y, z)}. \quad (48)$$

For a separable initial pulsed-beam input, $\Delta\chi_1^{(tot)}$ is given by Eq. (38). In addition, the t dependences of Ψ_{10} and $|\phi_1|$ are identical. Therefore, in this case, the dependence on t cancels out on the right hand side of Eq. (48), and $\Delta I_1^{(r)(1)}$ becomes independent of t . It follows that for a separable initial pulsed-beam input, the expression for $\Delta I_1^{(r)(1)}$ is:

$$\begin{aligned} \Delta I_1^{(r)}(x, y, z) &= -\frac{2|\phi_1(t, x, y, z)|}{A_1(0)\Psi_{10}(t, x, y, z)} \\ &\times \cos \left[\chi_{10}^{(x)}(x, z) + \chi_{10}^{(y)}(y, z) - \chi_1^{(x)}(x, z) - \chi_1^{(y)}(y, z) - \pi \right]. \end{aligned} \quad (49)$$

The form of the approximate expression for the intensity reduction factor at $z = z_c^+$ is of particular interest, since it is used for the design of collision setups that lead to strong intensity reduction effects. We therefore turn to obtain the expression for $\Delta I_1^{(r)(1)}(x, y, z_c^+)$. From Eq. (20) it follows that $|\phi_1(t, x, y, z_c^+)| = \Phi_1(t, x, y, z_c^+) = \Delta\Phi_1(t, x, y, z_c)$ and $\Delta\chi_1^{(tot)}(x, y, z_c^+) = 0$. Therefore, the expression for $\Delta I_1^{(r)(1)}(x, y, z_c^+)$ is

$$\Delta I_1^{(r)(1)}(x, y, z_c^+) = -\frac{2\Delta\Phi_1(t, x, y, z_c)}{A_1(0)\Psi_{10}(t, x, y, z_c)}. \quad (50)$$

When the initial pulsed-beam input is separable, we can express $\Delta\Phi_1$ by Eq. (30) and obtain:

$$\Delta I_1^{(r)(1)}(x, y, z_c^+) = \frac{4\epsilon_3 A_2^2(0)}{|\Delta\beta_1|} c_{p2}^{(t)} W_{20}^{(t)} G_2^{(x)2}(x, z_c) G_2^{(y)2}(y, z_c). \quad (51)$$

We take advantage of the simple form of Eq. (51), and use it to estimate the physical parameter values required for realizing strong collision-induced intensity reduction effects.

C. Design of the collision setups

The design of collision setups that lead to strong localized and nonlocalized intensity reduction effects is based on the simple form of Eq. (51). We employ this equation for the Gaussian initial condition (39) and obtain

$$\Delta I_1^{(r)(1)}(x, y, z_c^+) = \frac{4\pi^{1/2}\epsilon_3 A_2^2(0) W_{20}^{(t)} W_{20}^{(x)} W_{20}^{(y)}}{|\Delta\beta_1| W_2^{(x)}(z_c) W_2^{(y)}(z_c)} \exp \left[-\frac{x^2}{W_2^{(x)2}(z_c)} - \frac{y^2}{W_2^{(y)2}(z_c)} \right], \quad (52)$$

where the z -dependent pulsed-beam widths in the x and y directions are given by

$$W_j^{(x)}(z) = \left(W_{j0}^{(x)2} + \frac{4d_{2j}^2 z^2}{W_{j0}^{(x)2}} \right)^{1/2}, \quad W_j^{(y)}(z) = \left(W_{j0}^{(y)2} + \frac{4d_{2j}^2 z^2}{W_{j0}^{(y)2}} \right)^{1/2}. \quad (53)$$

Further simplification is obtained by calculating $\Delta I_1^{(r)}$ on the z axis. We obtain:

$$\Delta I_1^{(r)(1)}(0, 0, z_c^+) = \frac{4\pi^{1/2}\epsilon_3 A_2^2(0) W_{20}^{(t)} W_{20}^{(x)} W_{20}^{(y)}}{|\Delta\beta_1| W_2^{(x)}(z_c) W_2^{(y)}(z_c)}. \quad (54)$$

We now describe the main guiding principles that are used in the design of the collision setups that lead to strong intensity reduction effects.

1. We consider setups that lead to significant collision-induced intensity change but that are not completely outside of the region of validity of the perturbative calculation. We therefore require:

$$0.1 < \Delta I_1^{(r)(1)}(0, 0, z_c^+) < 1.0. \quad (55)$$

2. (a) For localized collision setups, we look for a generic case, in which the diffraction-induced broadening of pulsed-beam 2 at $z = z_c$ is not very large on one hand, and is not negligible on the other hand. We therefore require:

$$W_{20}^{(x)2} \gtrsim 2d_{22}z_c, \quad W_{20}^{(y)2} \gtrsim 2d_{22}z_c. \quad (56)$$

We then determine the value of d_{22} by using

$$d_{22} \approx W_{20}^{(x)2}/(2z_c), \quad d_{22} \approx W_{20}^{(y)2}/(2z_c). \quad (57)$$

We emphasize, however, that this condition is not very limiting, as somewhat smaller or larger values of d_{22} can be used.

- (b) For nonlocalized collision setups, we look for a generic case, in which the diffraction-induced broadening of both pulsed-beams at $z = z_c$ is not very large and not negligible.

3. Spatially localized reduction in the intensity of pulsed-beam 1 can be realized by requiring that

$$W_2^{(x)}(z_c) \ll W_1^{(x)}(z_c), \quad W_2^{(y)}(z_c) \ll W_1^{(y)}(z_c). \quad (58)$$

Using Eq. (53), we find that condition (58) can be satisfied by choosing

$$W_{20}^{(x)} \ll W_{10}^{(x)}, \quad W_{20}^{(y)} \ll W_{10}^{(y)}. \quad (59)$$

In a similar manner, nonlocalized intensity reduction for pulsed-beam 1 can be realized by taking

$$W_{20}^{(x)} \approx W_{10}^{(x)}, \quad W_{20}^{(y)} \approx W_{10}^{(y)}. \quad (60)$$

IV. NUMERICAL SIMULATIONS

The predictions of the previous sections are based on a number of simplifying approximations, and the validity conditions for these approximations are not known. For example, it is unclear if the approximation of $\Psi_{20}(t, x, y, z)$ by $\bar{\Psi}_{20}(\tilde{t}, x, y, z_c)$, which was used in the derivation of Eq. (15) from Eq. (14), is valid under the conditions specified in the end of subsection II A. Moreover, in the current paper, we develop and study collision setups that lead to relatively strong intensity reduction effects. For these setups, the validity of the entire perturbative calculation might break down. For this reason, it is important to check the perturbation theory predictions by numerical simulations with Eq. (5). In the current paper, we take on this important investigation. More specifically, we carry out numerical simulations with Eq. (5) for two collision setups, one that leads to strong localized intensity reduction effects (section IV A), and another that leads to strong nonlocalized intensity reduction effects (section IV B). In both cases, we numerically solve Eq. (5) with the initial condition (39) by the split-step method with periodic boundary conditions [12, 59]. Furthermore, we compare the simulations results with the approximate predictions of the perturbation theory.

A. A collision setup with localized effects

We start by considering collision setup 1, which leads to strong spatially localized intensity reduction effects. The main conditions that guide the choice of the physical parameter values

for this setup are specified by Eqs. (54), (55), (57), and (59). We use these conditions in the following manner.

1. Spatially localized intensity reduction for pulsed-beam 1 is realized by choosing $W_{10}^{(x)} = W_{10}^{(y)} = 5$ and $W_{20}^{(x)} = W_{20}^{(y)} = 0.5$, in accordance with condition (59).
2. We choose $t_{10} = 0$ and $t_{20} = -20$, such that the pulsed-beams are well-separated at $z = 0$. In addition, $\Delta\beta_1 = 10$, and as a result, the collision distance is $z_c = 2$. Using condition (57), we find that $d_{22} \approx 0.0625$, so we choose $d_{22} = 0.06$.
3. From the relations $d_{2j} = \tau_0^2 \lambda_j / (2\pi |\tilde{\beta}_{21}| x_0'^2)$ in Eq. (6), it follows that $d_{21} = \lambda_1 d_{22} / \lambda_2$. For a realistic choice of the wavelengths (see below), λ_1 is close to λ_2 , and as a result, $d_{21} \approx d_{22}$. We therefore use $d_{21} = 0.06$.
4. Using Eq. (53) with the parameter values specified in the previous items, we find $W_2^{(x)}(z_c) = W_2^{(y)}(z_c) \simeq 0.693$, and $W_1^{(x)}(z_c) = W_1^{(y)}(z_c) \simeq 5.000$. Therefore, condition (58) is satisfied for the chosen parameter values.
5. Strong intensity reduction effects are realized by choosing $\epsilon_3 = 0.12$, $A_2(0) = 2$, and $W_{20}^{(t)} = 5$, in accordance with Eqs. (54) and (55). With this choice we obtain $\Delta I_1^{(r)(1)}(0, 0, z_c^+) \simeq 0.886$.
6. The values of the other physical parameters are taken as $\beta_{22} = 1$, $A_1(0) = 1$, and $W_{10}^{(t)} = 1$. Additionally, the final propagation distance is chosen as $z_f = 2z_c = 4$, such that the pulsed-beams are also well-separated at $z = z_f$.

Let us provide an example for the values of the dimensional physical parameters that correspond to the values of the dimensionless parameters specified in items 1-6. For this purpose, we consider bulk fused silica as an example for the optical medium. We use the information in Refs. [60, 61] and choose $x_0' = 2$ cm, $\lambda_1 = 2.791$ μm , $\lambda_2 = 2.795$ μm , $\tilde{\beta}_{21} = -394.23$ $\text{ps}^2\text{km}^{-1}$, $\tilde{\beta}_{22} = -396.59$ $\text{ps}^2\text{km}^{-1}$, $\tilde{d}_{21} = 2.221 \times 10^{-7}$ m, $\tilde{d}_{22} = 2.224 \times 10^{-7}$ m, $\tau_0 = 4.615$ ps, $P_0 = 0.05$ W, $\rho_3 = 22.210$ $\text{W}^{-1}\text{km}^{-1}$, and $z_c'' = 216.0$ m [62].

We now turn to describe the results of the numerical simulation. Figure 1 shows the pulsed-beam shapes $|\psi_j(t, x, y, z)|$ obtained in the simulation at three specific planes (cross-sections) at distance $z = 0$, the intermediate distance $z = z_i = 2.4$, and the final distance $z = z_f = 4.0$ [63, 64]. We observe that the pulsed-beams experience broadening due to the

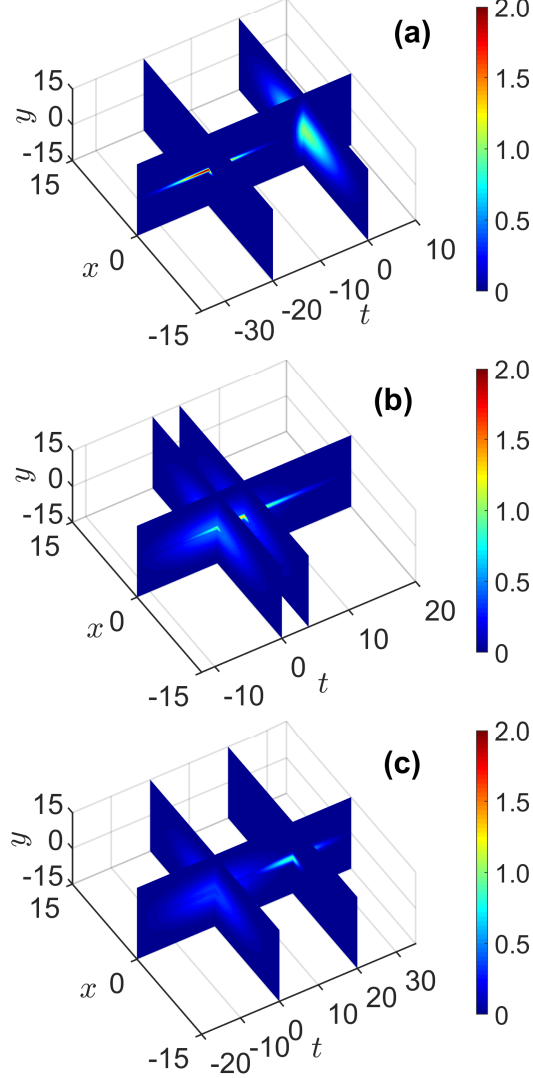


FIG. 1: (Color online) Contour plots of the pulsed-beam shapes $|\psi_j(t, x, y, z)|$ on three planes in the txy space at $z = 0$ (a), $z = z_i = 2.4$ (b), and $z = z_f = 4.0$ (c) in a fast collision with strong spatially localized effects (collision setup 1). The cubic loss coefficient is $\epsilon_3 = 0.12$ and the first-order dispersion coefficient is $\Delta\beta_1 = 10$. The plots represent the pulsed-beam shapes obtained by numerical solution of Eq. (5) with the initial condition (39). The three planes are $x = 0$, $t = 0$, and $t = t_2(z)$ with $z = 0$, $z = z_i$, and $z = z_f$ in (a), (b), and (c), respectively.

effects of second-order dispersion and diffraction. Furthermore, the values of $|\psi_j(t, x, y, z)|$ in the main bodies of the pulsed-beams decrease significantly. We further characterize the intensity decrease for pulsed-beam 1 by presenting the graphs of $|\psi_1(0, x, y, z)|$ vs x and y at $z = 0$, $z = z_i$, and $z = z_f$ in Fig. 2. It is seen that the intensity decrease is a result of both

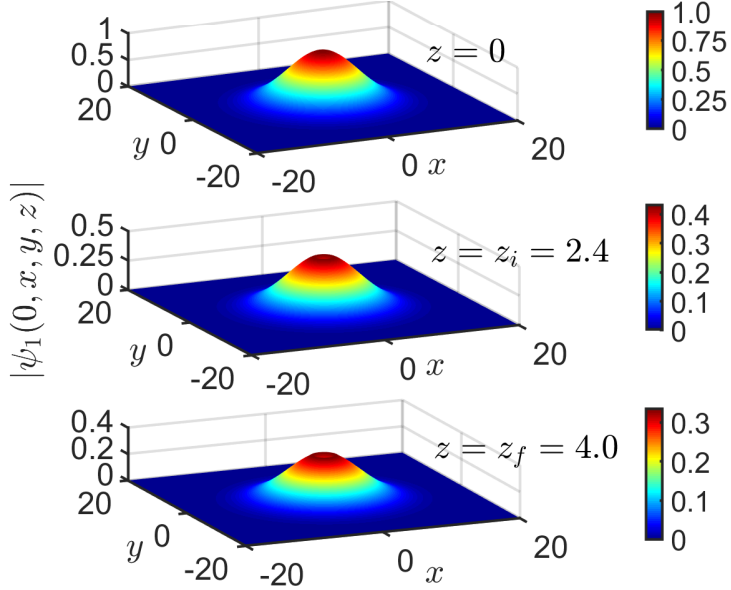


FIG. 2: (Color online) The shape of pulsed-beam 1 at $t = 0$ $|\psi_j(0, x, y, z)|$ vs x and y at $z = 0$ (top), $z = z_i = 2.4$ (middle), and $z = z_f = 4.0$ (bottom) in a fast two-beam collision with strong spatially localized effects. The parameter values are the same as in Fig. 1. The plots represent the shape of pulsed-beam 1 obtained by numerical solution of Eq. (5) with the initial condition (39).

dispersion-induced (and diffraction-induced) broadening and the relatively strong effect of cubic loss on the collision. Moreover, the intensity reduction is spatially localized near the z axis, and it leads to the generation of a local minimum in the graph of $|\psi_1(0, x, y, z)|$ vs x and y on the z axis.

The validity of the perturbation theory prediction for the collision-induced change in the shape of pulsed-beam 1 $\phi_j(t, x, y, z)$ is checked in Fig. 3. More specifically, this figure shows a comparison between the theoretical prediction of Eq. (44) $|\phi_1^{(th)}(t, x, y, z)|$ and the numerical simulation's result $|\phi_1^{(num)}(t, x, y, z)|$ at $z = z_f$. We observe that the magnitude of the collision-induced change in the pulsed-beam's shape is much larger than the one observed in the collision setups considered in Ref. [28] for time-independent optical beams, and in Ref. [39] for conventional optical solitons in dimension 1. (Compare Fig. 3 with Fig. 7 in Ref. [28] and with Fig. 1 in Ref. [39]). Furthermore, despite the relatively strong collision-induced changes seen in Fig. 3, the agreement between the theoretical prediction and the simulation's result is good. We quantify the deviation of $|\phi_1^{(th)}(t, x, y, z)|$ from

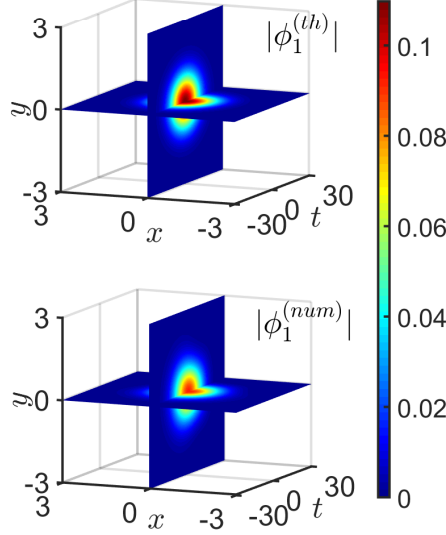


FIG. 3: (Color online) The collision-induced change in the shape of pulsed-beam 1 $|\phi_1(t, x, y, z_f)|$ at $z_f = 4.0$ in a fast two-beam collision with parameter values $\epsilon_3 = 0.12$ and $\Delta\beta_1 = 10$ (collision setup 1). Top: the perturbation theory prediction of Eq. (44). Bottom: the result obtained by numerical solution of Eq. (5).

$|\phi_1^{(num)}(t, x, y, z)|$ by defining the relative error (in percentage) $E_r^{(\phi_1)}(z)$ as

$$E_r^{(\phi_1)}(z) = 100 \times \left[\int dt \int dx \int dy |\phi_1^{(th)}(t, x, y, z)|^2 \right]^{-1/2} \times \left\{ \int dt \int dx \int dy \left[\left| \phi_1^{(th)}(t, x, y, z) \right| - \left| \phi_1^{(num)}(t, x, y, z) \right| \right]^2 \right\}^{1/2}, \quad (61)$$

where the integration is performed over the entire simulation domain. The calculated value of $E_r^{(\phi_1)}(z_f)$ for the collision setup considered here is 17.5%, in accordance with the good agreement between theory and simulation observed in Fig. 3.

Important insight into the collision-induced effects is gained by analyzing the behavior of the fractional intensity reduction factor $\Delta I_1^{(r)}(x, y, z)$. The dependence of the intensity reduction factor on x and y at $z = z_f$ that was obtained in the simulation with Eq. (5) $\Delta I_1^{(r)(num)}$ is shown in Fig. 4(a) [65]. The perturbation theory prediction of Eq. (49) $\Delta I_1^{(r)(1)}$ is shown in Fig. 4(b). We observe good agreement between the two results. In particular, the values of $\Delta I_1^{(r)(num)}$ are larger than 0.25 within a disk of radius $R \simeq 0.8$, which is much smaller than the initial pulsed-beam width $W_{10}^{(x)} = W_{10}^{(y)} = 5$, in accordance with the perturbation theory prediction for strong localized intensity reduction effects. We

also note that the perturbation theory prediction overestimates the values of the intensity reduction factor in the main body of the pulsed-beam. For example, the maximal values of $\Delta I_1^{(r)(1)}$ and $\Delta I_1^{(r)(num)}$, which are attained at $R \approx 0.1$ and $R \approx 0.3$, are 0.443 and 0.319, respectively. We further quantify the deviation of $\Delta I_1^{(r)(1)}$ from $\Delta I_1^{(r)(num)}$ by defining the relative error $E_r^{(\Delta I_1^{(r)(1)})}(z)$ (in percentage):

$$E_r^{(\Delta I_1^{(r)(1)})}(z) = 100 \times \left[\int dx \int dy |\Delta I_1^{(r)(1)}(x, y, z)|^2 \right]^{-1/2} \times \left\{ \int dx \int dy \left[\left| \Delta I_1^{(r)(1)}(x, y, z) \right| - \left| \Delta I_1^{(r)(num)}(x, y, z) \right| \right]^2 \right\}^{1/2}. \quad (62)$$

The value of $E_r^{(\Delta I_1^{(r)(1)})}(z_f)$ for the current collision setup is 23.6%, which is consistent with the comparison shown in Fig. 4.

The deviation of $\Delta I_1^{(r)(1)}$ from $\Delta I_1^{(r)(num)}$ is clearly associated with the strong effects of the collision. Therefore, one can expect that better agreement between theory and simulation would be obtained by including effects of order higher than $\epsilon_3/|\Delta\beta_1|$ in the perturbative calculation of $\Delta I_1^{(r)}$. In the current paper we do not carry out the full calculation of high-order contributions to $\Delta I_1^{(r)}$, since as we will see below, this lengthy calculation is not essential for obtaining significant improvement in the agreement between theory and simulation. Instead, we add only the correction to $\Delta I_1^{(r)}$ due to the $O(\epsilon_3^2/|\Delta\beta_1|^2)$ contribution from the term $-|\phi_1|^2/(A_1^2(0)\Psi_{10}^2)$. Consequently, the improved prediction for the intensity reduction factor $\Delta I_1^{(r)(2)}$ is given by:

$$\Delta I_1^{(r)(2)}(x, y, z) = -\frac{2|\phi_1(t, x, y, z)| \cos \left[\Delta\chi_1^{(tot)}(t, x, y, z) \right]}{A_1(0)\Psi_{10}(t, x, y, z)} - \frac{|\phi_1(t, x, y, z)|^2}{A_1^2(0)\Psi_{10}^2(t, x, y, z)}. \quad (63)$$

The comparison between $\Delta I_1^{(r)(2)}$ and $\Delta I_1^{(r)(num)}$ is shown in the bottom row of Fig. 4. It is seen that the agreement between the two results is significantly better than the agreement between $\Delta I_1^{(r)(1)}$ and $\Delta I_1^{(r)(num)}$. Accordingly, the relative error (in percentage) in the approximation of the intensity reduction factor by $\Delta I_1^{(r)(2)}$, $E_r^{(\Delta I_1^{(r)(2)})}(z)$, which is defined by an equation similar to Eq. (62), is only 13.4% at $z = z_f$. Thus, the introduction of the term $-|\phi_1|^2/(A_1^2(0)\Psi_{10}^2)$ does lead to significant improvement in the accuracy of the perturbation theory prediction. It follows that the relatively strong intensity reduction effects observed in the current collision setup can be correctly explained by using only the leading-order term in the expansion of ϕ_1 (i.e., the term of order $\epsilon_3/|\Delta\beta_1|$). This finding is important since it

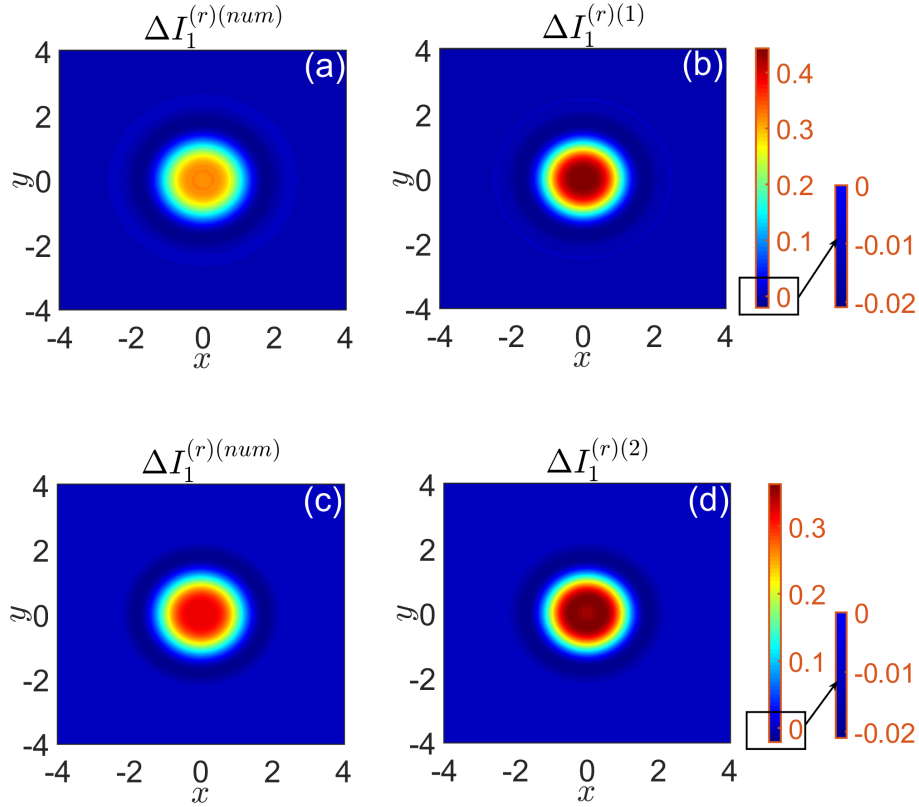


FIG. 4: (Color online) The fractional intensity reduction factor for pulsed-beam 1 $\Delta I_1^{(r)}(x, y, z)$ vs x and y at $z = z_f$ in a fast two-beam collision with parameter values $\epsilon_3 = 0.12$ and $\Delta\beta_1 = 10$ (collision setup 1). The result obtained in the simulation with Eq. (5) is shown in (a) and (c). The perturbation theory predictions of Eqs. (49) and (63) are shown in (b) and (d), respectively.

means that the design of the collision setups that are considered in the current paper, which lead to significant intensity reduction effects, can indeed be based on the relatively simple calculation of ϕ_1 in the leading order of the perturbative calculation.

To gain further understanding of the effects of cubic loss on fast collisions we investigate the dependences of $\Delta I_1^{(r)}(0, 0, z_f)$ (the value of the intensity reduction factor on the z axis) and $\Delta A_1^{(c)}$ (the collision-induced amplitude shift) on the first-order dispersion coefficient $\Delta\beta_1$. For this purpose, we carry out extensive numerical simulations with Eq. (5) with the parameter values specified in the beginning of the current subsection and with $\Delta\beta_1$ values in the intervals $6 \leq |\Delta\beta_1| \leq 60$. We denote the values of $\Delta I_1^{(r)}(0, 0, z_f)$ and $\Delta A_1^{(c)}$ obtained in the simulations by $\Delta I_1^{(r)(num)}(0, 0, z_f)$ and $\Delta A_1^{(c)(num)}$, respectively. Figure 5 shows the

dependence of $\Delta I_1^{(r)(num)}(0, 0, z_f)$ on $\Delta\beta_1$ along with the perturbation theory predictions of Eqs. (49) and (63), $\Delta I_1^{(r)(1)}(0, 0, z_f)$ and $\Delta I_1^{(r)(2)}(0, 0, z_f)$. We first note that the values of $\Delta I_1^{(r)(num)}(0, 0, z_f)$ are larger than 0.2 over the entire $\Delta\beta_1$ intervals, in accordance with the perturbation theory predictions for strong intensity reduction. We also note that these values are larger by two orders of magnitude compared with the values obtained in Ref. [28] for fast collisions between time-independent beams. Another interesting feature seen in Fig. 5 is that $\Delta I_1^{(r)(num)}(0, 0, z_f)$ has two local maxima at $\Delta\beta_1 \approx \pm 20.0$. These local maxima are correctly captured by the perturbation theory prediction $\Delta I_1^{(r)(2)}$ but not by $\Delta I_1^{(r)(1)}$. More generally, we observe good agreement between $\Delta I_1^{(r)(1)}(0, 0, z_f)$ and $\Delta I_1^{(r)(num)}(0, 0, z_f)$ and very good agreement between $\Delta I_1^{(r)(2)}(0, 0, z_f)$ and $\Delta I_1^{(r)(num)}(0, 0, z_f)$ over the entire $\Delta\beta_1$ intervals. Importantly, the agreement between the two theoretical results and the simulations result improves with increasing value of $|\Delta\beta_1|$. Therefore, the collision setup considered in the current subsection leads to significant intensity reduction effects not only for intermediate values of $|\Delta\beta_1|$, but also for large $|\Delta\beta_1|$ values. Note that the collision distance z_c is inversely proportional to $|\Delta\beta_1|$. Therefore, the latter finding means that significant intensity reduction effects can also be observed at much shorter distances than the dimensional collision distance $z_c'' = 216.0$ m of the collision setup with $\Delta\beta_1 = 10$. For example, for $\Delta\beta_1 = 50$, the dimensional collision distance is only $z_c'' = 43.2$ m, and the value of $\Delta I_1^{(r)(num)}(0, 0, z_f)$ is 0.248.

The dependence of the collision-induced amplitude shift $\Delta A_1^{(c)}$ on $\Delta\beta_1$ that is obtained in the simulations is shown in Fig. 6 together with the perturbation theory prediction of Eq. (45). We observe good agreement between the perturbation theory and the simulations over the entire $\Delta\beta_1$ intervals despite the strong intensity reduction effects. More specifically, the relative error in the approximation of $\Delta A_1^{(c)}$ (in percentage), which is defined by $E_r = 100|\Delta A_1^{(c)(num)} - \Delta A_1^{(c)(th)}|/|\Delta A_1^{(c)(th)}|$, is smaller than 19.4% for $6 \leq |\Delta\beta_1| < 30$ and smaller than 12.2% for $30 \leq |\Delta\beta_1| \leq 60$. Therefore, the perturbative calculation that is used to design the collision setups that lead to strong intensity reduction effects also correctly captures the behavior of the collision-induced amplitude shift. We also observe that the values of $\Delta A_1^{(c)(num)}$ in Fig. 6 are smaller by one to two orders of magnitude compared with the values of $\Delta I_1^{(r)(num)}(0, 0, z_f)$ in Fig. 5. This can be explained by noting that $\Delta I_1^{(r)}$ is a measure for localized intensity changes. In contrast, $\Delta A_1^{(c)}$ is a measure for global (total) intensity changes, since its calculation involves integration over the spatial coordinates [see

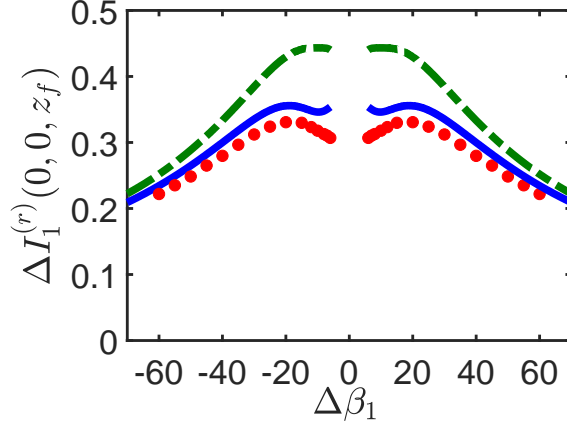


FIG. 5: (Color online) The fractional intensity reduction factor for pulsed-beam 1 at $(x, y) = (0, 0)$ and $z = z_f$, $\Delta I_1^{(r)}(0, 0, z_f)$, vs the first-order dispersion coefficient $\Delta\beta_1$ in fast two-beam collisions with $\epsilon_3 = 0.12$ (collision setup 1). The red circles represent the result obtained by numerical simulations with Eq. (5). The dashed-dotted green and solid blue curves correspond to the perturbation theory predictions of Eqs. (49) and (63), respectively.

Eqs. (18) and (31)]. In the current setup, the strong intensity reduction effects are localized in a small region near the z axis (see the discussion of Fig. 4). As a result, this strong but spatially localized intensity reduction leads only to relatively small amplitude shifts. In the next subsection, we consider a collision setup with nonlocalized intensity reduction effects, for which the values of both $\Delta A_1^{(c)(num)}$ and $\Delta I_1^{(r)(num)}(0, 0, z_f)$ are relatively large.

B. A collision setup with nonlocalized effects

We now turn to discuss collision setup 2, which leads to strong but nonlocalized intensity reduction effects. It is interesting to consider this second setup, since some important features of the collision-induced effects in this case are very different from the ones observed for collision setup 1. The values of the physical parameters for setup 2 are chosen by using the conditions (54), (55), and (60) in the following manner.

1. Nonlocalized intensity reduction for pulsed-beam 1 is realized by choosing $W_{10}^{(x)} = W_{10}^{(y)} = 3$ and $W_{20}^{(x)} = W_{20}^{(y)} = 2$, in accordance with condition (60).
2. We choose $t_{10} = 0$ and $t_{20} = -20$, such that the pulsed-beams are well-separated

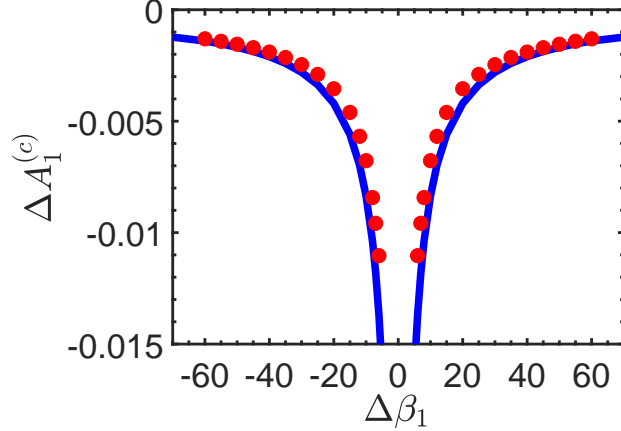


FIG. 6: (Color online) The collision-induced amplitude shift of pulsed-beam 1 $\Delta A_1^{(c)}$ vs the first-order dispersion coefficient $\Delta\beta_1$ in fast two-beam collisions with $\epsilon_3 = 0.12$ (collision setup 1). The red circles represent the result obtained by numerical simulations with Eq. (5). The solid blue curve represents the perturbation theory prediction of Eq. (45).

at $z = 0$. We also choose $\Delta\beta_1 = 20$, and therefore, $z_c = 1$. The value of d_{21} is chosen as 1.0, and therefore, the diffraction-induced broadening of pulsed-beam 1 is nonnegligible at $z = z_c$.

3. Since λ_1 is close to λ_2 , it follows from the relation $d_{22} = \lambda_2 d_{21} / \lambda_1$ that $d_{22} \approx d_{21}$. We therefore use $d_{22} = 1.0$. As a result, the diffraction-induced broadening of pulsed-beam 2 at $z = z_c$ is also nonnegligible.
4. Strong intensity reduction effects are realized by choosing $\epsilon_3 = 0.25$, $A_2(0) = 1.3$, and $W_{20}^{(t)} = 5$, in conformity with Eqs. (54) and (55). This choice yields $\Delta I_1^{(r)(1)}(0, 0, z_c^+) \simeq 0.599$.
5. The other physical parameters values are taken as $\beta_{22} = 1$, $A_1(0) = 1$, and $W_{10}^{(t)} = 1$. In addition, $z_f = 2z_c = 2$, such that the pulsed-beams are also well-separated at $z = z_f$.

It is useful to provide an example for the values of the dimensional physical parameters that correspond to the values of the dimensionless parameters in items 1-5. Considering bulk fused silica as an example for the optical medium and using the information in Refs. [60, 61], we find the following values. $x'_0 = 2$ cm, $\lambda_1 = 2.791$ μm , $\lambda_2 = 2.795$ μm , $\tilde{\beta}_{21} = -394.23$

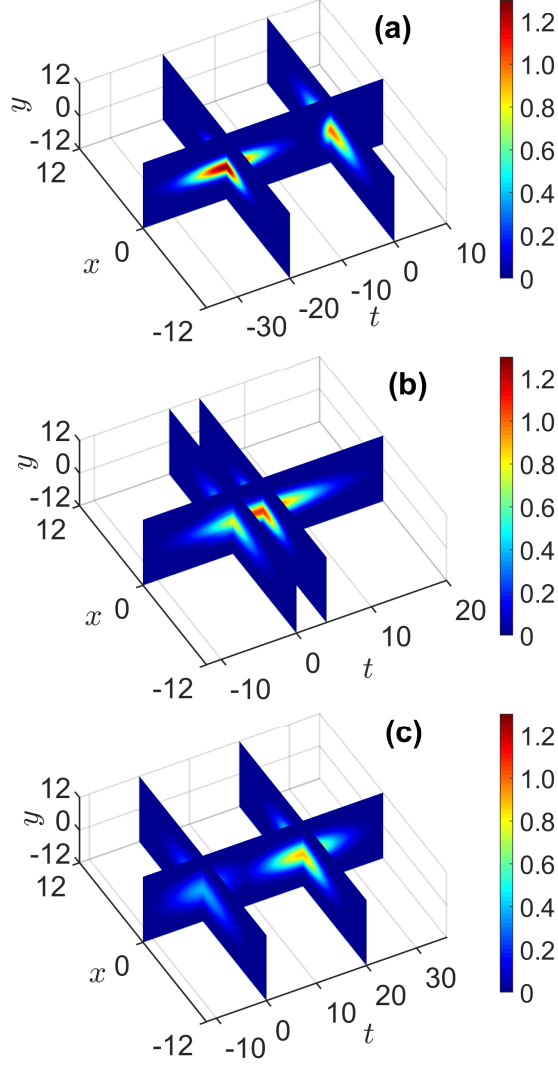


FIG. 7: (Color online) Contour plots of the pulsed-beam shapes $|\psi_j(t, x, y, z)|$ on three planes in the txy space at $z = 0$ (a), $z = z_i = 1.2$ (b), and $z = z_f = 2.0$ (c) in a fast collision with strong but nonlocalized effects (collision setup 2). The cubic loss coefficient is $\epsilon_3 = 0.25$ and the first-order dispersion coefficient is $\Delta\beta_1 = 20$. The plots represent the pulsed-beam shapes obtained by numerical solution of Eq. (5) with the initial condition (39). The three planes are $x = 0$, $t = 0$, and $t = t_2(z)$ with $z = 0$, $z = z_i$, and $z = z_f$ in (a), (b), and (c), respectively.

$\text{ps}^2\text{km}^{-1}$, $\tilde{\beta}_{22} = -396.59 \text{ ps}^2\text{km}^{-1}$, $\tilde{d}_{21} = 2.221 \times 10^{-7}\text{m}$, $\tilde{d}_{22} = 2.224 \times 10^{-7}\text{m}$, $\tau_0 = 9.421 \text{ ps}$, $P_0 = 0.05 \text{ W}$, $\rho_3 = 11.104 \text{ W}^{-1}\text{km}^{-1}$, and $z_c'' = 450.2 \text{ m}$ [66].

Let us describe the results of the numerical simulation for collision setup 2. Figure 7 shows the pulsed-beam shapes $|\psi_j(t, x, y, z)|$ obtained in the simulation at three specific

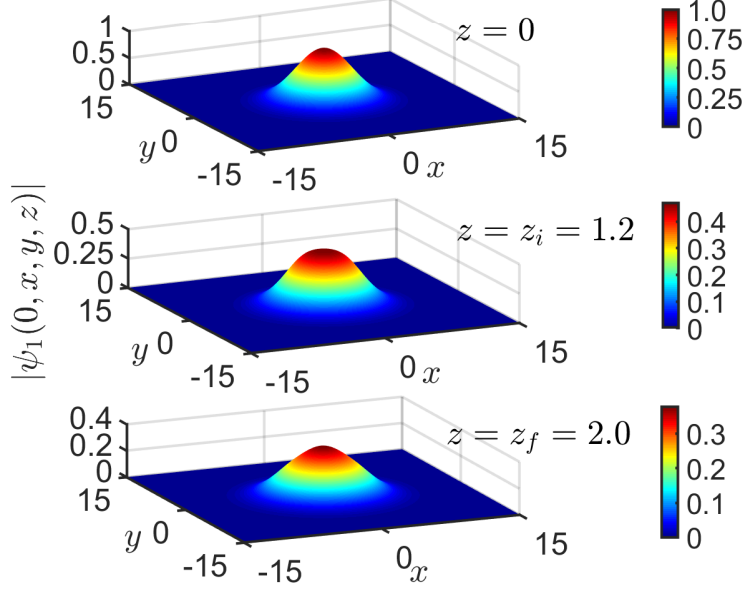


FIG. 8: (Color online) The shape of pulsed-beam 1 at $t = 0$ $|\psi_j(0, x, y, z)|$ vs x and y at $z = 0$ (top), $z = z_i = 1.2$ (middle), and $z = z_f = 2.0$ (bottom) in a fast two-beam collision with strong but nonlocalized effects. The parameter values are the same as in Fig. 7. The plots represent the shape of pulsed-beam 1 obtained by the numerical simulation with Eq. (5) with the initial condition (39).

planes at the distances $z = 0$, $z = z_i = 1.2$, and $z = z_f = 2.0$. It is seen that the pulsed-beams broaden due to both second-order dispersion and diffraction. Additionally, the values of $|\psi_j(t, x, y, z)|$ in the main bodies of the pulsed-beams decrease significantly. The intensity decrease of pulsed-beam 1 is further characterized in Fig. 8, which shows the graphs of $|\psi_1(0, x, y, z)|$ vs x and y at $z = 0$, $z = z_i$, and $z = z_f$. We observe that the intensity decrease of pulsed-beam 1 is a result of the interplay between dispersion-induced and diffraction-induced beam broadening and the strong effect of cubic loss on the collision. Furthermore, in contrast to the situation in setup 1, the intensity decrease is not localized in a small region near the z axis, but affects the whole main body of the pulsed-beam.

The nonlocalized character of the collisional effects is also seen in Fig. 9, which shows a comparison between the theoretical and numerical results for the collision-induced change in the shape of pulsed-beam 1 at $z = z_f$, $|\phi_1^{(th)}(t, x, y, z_f)|$ and $|\phi_1^{(num)}(t, x, y, z_f)|$. More specifically, the values of $|\phi_1^{(num)}(t, x, y, z_f)|$ in Fig. 9 are larger than 0.07 in a ball of radius $R \approx 1.3$, whereas the $|\phi_1^{(num)}(t, x, y, z_f)|$ values in Fig. 3 are larger than 0.07 in a ball

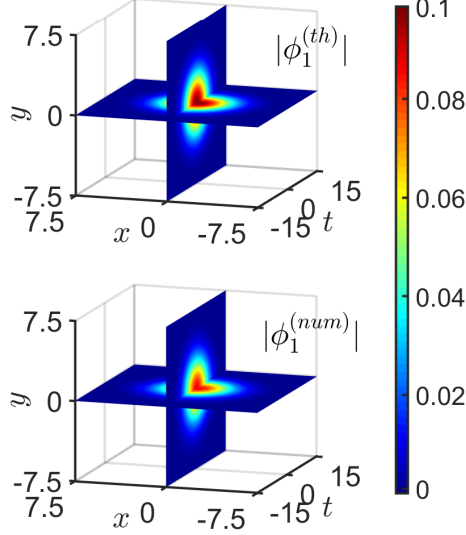


FIG. 9: (Color online) The collision-induced change in the shape of pulsed-beam 1 $|\phi_1(t, x, y, z_f)|$ at $z_f = 2.0$ in a fast two-beam collision with parameter values $\epsilon_3 = 0.25$ and $\Delta\beta_1 = 20$ (collision setup 2). Top: the perturbation theory prediction of Eq. (44). Bottom: the result obtained by numerical solution of Eq. (5).

whose radius is only $R \approx 0.5$. Moreover, we find that the agreement between the theoretical prediction and the numerical simulation's result for ϕ_1 in setup 2 is good despite the relatively strong effects of the collision. In particular, the relative error $E_r^{(\phi_1)}(z_f)$, which is calculated with Eq. (61), is only 13.2%. We also observe that the maximal value of $|\phi_1^{(num)}(t, x, y, z_f)|$ in setup 2 is of the same order of magnitude as in setup 1. Thus, the magnitude of the collision-induced change in the pulsed-beam's shape in setup 2 is also much larger than the one observed in Refs. [28] and [39] for fast collisions between time-independent optical beams and for fast collisions between optical solitons in dimension 1, respectively.

To gain further insight into the collision dynamics we analyze the behavior of the fractional intensity reduction factor. Figure 10(a) shows the dependence of $\Delta I_1^{(r)(num)}$ on x and y at $z = z_f$ [65], and Fig. 10(b) shows the perturbation theory prediction of Eq. (49) $\Delta I_1^{(r)(1)}$. We observe that unlike the situation in setup 1, the intensity reduction in setup 2 is nonlocalized and affects the entire main body of pulsed-beam 1. More specifically, the values of $\Delta I_1^{(r)(num)}$ are larger than 0.25 inside a disk of radius $R \approx 2.2$, which is close to the initial pulsed-beam width $W_{10}^{(x)} = W_{10}^{(y)} = 3$, and larger than the value obtained in setup 1. We also observe good agreement between $\Delta I_1^{(r)(1)}$ and $\Delta I_1^{(r)(num)}$. Indeed, the value of the relative

error $E_r^{(\Delta I_1^{(r)(1)})}(z_f)$ that is calculated with Eq. (62) is 18.6%, which is smaller than the value obtained in setup 1. Further improvement in the agreement between the theoretical and the numerical results is obtained by employing the perturbation theory prediction $\Delta I_1^{(r)(2)}$, which is defined by Eq. (63). The comparison between $\Delta I_1^{(r)(2)}$ and $\Delta I_1^{(r)(num)}$ is shown in Figs. 10(c) and 10(d). We observe that the agreement between $\Delta I_1^{(r)(2)}$ and $\Delta I_1^{(r)(num)}$ is considerably better than the agreement between $\Delta I_1^{(r)(1)}$ and $\Delta I_1^{(r)(num)}$. In accordance with the latter observation, the value of the relative error $E_r^{(\Delta I_1^{(r)(2)})}(z_f)$ is only 11.9%. Thus, based on the results shown in Figs. 3, 4, 9, and 10 and similar results obtained with other values of the physical parameters, we conclude that our perturbation approach can indeed be used to design collision setups that lead to strong localized and nonlocalized intensity reduction effects.

Since we are interested in the effects of cubic loss on fast collisions, it is important to study the dependence of the different collisional effects on $\Delta\beta_1$. We therefore carry out extensive numerical simulations with Eq. (5) with the parameter values mentioned in the beginning of this subsection and with $\Delta\beta_1$ values in the intervals $4 \leq |\Delta\beta_1| \leq 60$. We measure the final value of the intensity reduction factor on the z axis $\Delta I_1^{(r)}(0, 0, z_f)$ and the collision-induced amplitude shift $\Delta A_1^{(c)}$ as functions of $\Delta\beta_1$. Figure 11 shows the $\Delta\beta_1$ dependence of $\Delta I_1^{(r)}(0, 0, z_f)$ obtained in the simulations together with the two perturbation theory predictions of Eqs. (49) and (63). Similar to the situation in setup 1, the values of $\Delta I_1^{(r)(num)}(0, 0, z_f)$ are larger than 0.19 over the entire $\Delta\beta_1$ intervals, in agreement with the perturbation theory predictions for strong intensity reduction. We also observe that $\Delta I_1^{(r)}(0, 0, z_f)$ has two local maxima at $\Delta\beta_1 \approx \pm 7.0$, and that these local maxima are correctly captured by the two predictions of the perturbation theory. More generally, we find very good agreement between $\Delta I_1^{(r)(2)}(0, 0, z_f)$ and $\Delta I_1^{(r)(num)}(0, 0, z_f)$ and good agreement between $\Delta I_1^{(r)(1)}(0, 0, z_f)$ and $\Delta I_1^{(r)(num)}(0, 0, z_f)$ over the entire $\Delta\beta_1$ intervals. Furthermore, the agreement between the two theoretical predictions and the simulations result improves with increasing value of $|\Delta\beta_1|$. Therefore, based on the results seen in Fig. 11, we conclude that the significant intensity reduction effects in setup 2 are not limited to intermediate values of $|\Delta\beta_1|$, but are also observed for large $|\Delta\beta_1|$ values.

Figure 12 shows the $\Delta\beta_1$ dependence of $\Delta A_1^{(c)}$ that is obtained in the numerical simulations together with the perturbation theory prediction of Eq. (45). We first observe that

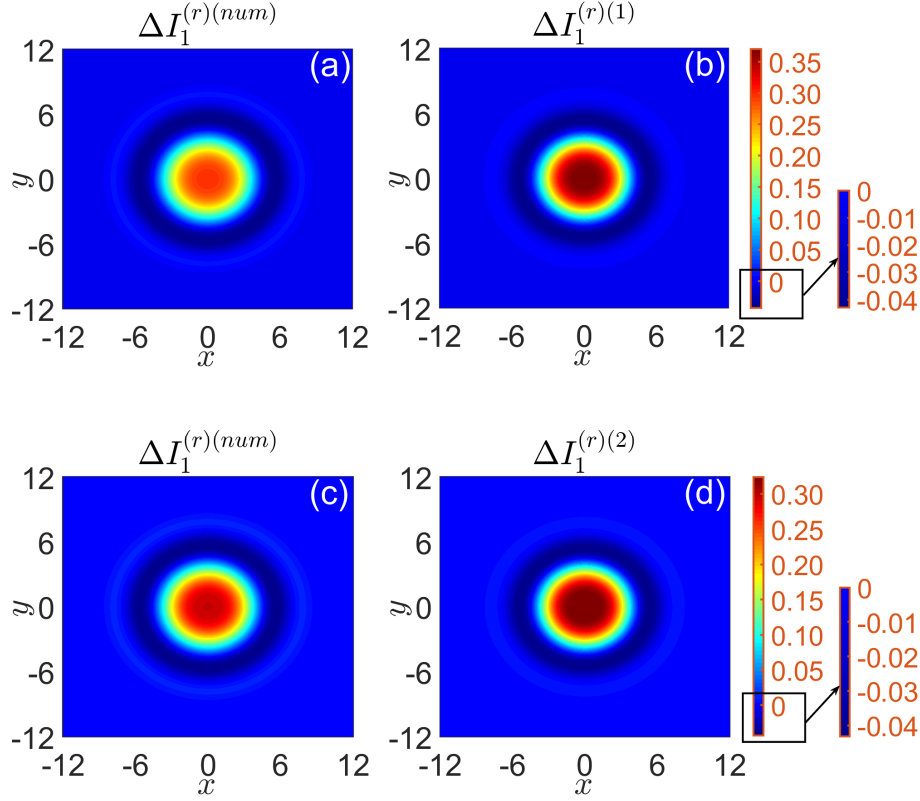


FIG. 10: (Color online) The fractional intensity reduction factor for pulsed-beam 1 $\Delta I_1^{(r)}(x, y, z)$ vs x and y at $z = z_f$ in a fast two-beam collision with parameter values $\epsilon_3 = 0.25$ and $\Delta\beta_1 = 20$ (collision setup 2). The result obtained by numerical solution of Eq. (5) is shown in (a) and (c). The perturbation theory predictions of Eqs. (49) and (63) are shown in (b) and (d), respectively.

the values of $\Delta A_1^{(c)(num)}$ are of orders $10^{-2} - 10^{-1}$, and are larger by one to two orders of magnitude compared with the $\Delta A_1^{(c)(num)}$ values in setup 1. This behavior can be explained by the difference in the nature of the intensity reduction in the two setups; the intensity reduction is nonlocalized in setup 2 and localized in setup 1. As a result, the values of $\Delta A_1^{(c)}$, which are a measure for global intensity changes, are significantly larger in setup 2 compared with setup 1. We also observe good agreement between $\Delta A_1^{(c)(num)}$ and the theoretical prediction of Eq. (45). In particular, the relative error in the approximation of $\Delta A_1^{(c)}$ is smaller than 19.7% for $4 \leq |\Delta\beta_1| < 30$ and smaller than 10.5% for $30 \leq |\Delta\beta_1| \leq 60$. Thus, the dependence of $\Delta A_1^{(c)}$ on $\Delta\beta_1$ is correctly captured by our perturbation approach despite the strong collision-induced effects.

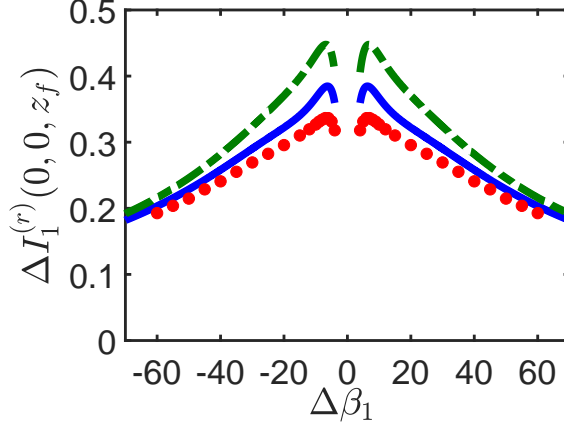


FIG. 11: (Color online) The fractional intensity reduction factor for pulsed-beam 1 at $(x, y) = (0, 0)$ and $z = z_f$, $\Delta I_1^{(r)}(0, 0, z_f)$, vs the first-order dispersion coefficient $\Delta\beta_1$ in fast two-beam collisions with $\epsilon_3 = 0.25$ (collision setup 2). The red circles represent the result obtained by numerical simulations with Eq. (5). The dashed-dotted green and solid blue curves represent the perturbation theory predictions of Eqs. (49) and (63), respectively.

Another important feature of the collision effects that is seen in Fig. 12 is the existence of two local minima in the graph of $\Delta A_1^{(c)}$ vs $\Delta\beta_1$. The local minima are located at $\Delta\beta_1 \approx \pm 7.0$, and are correctly captured by the perturbation theory prediction of Eq. (45). In fact, using Eq. (45) with $d_{21} = d_{22} = d_2$, we can show that $\Delta A_1^{(c)}$ has two local minima at $\Delta\beta_1 = \pm 2t_{20}d_2(W_{10}^{(x)}W_{10}^{(y)}W_{20}^{(x)}W_{20}^{(y)})^{-1/2}$. Using the latter relation with the parameter values of setup 2, we obtain $\Delta\beta_1 \approx \pm 6.67$, in good agreement with the simulations result. We emphasize that to our knowledge, this result represents the first observation of a deviation of the graph of $\Delta A_1^{(c)}$ vs $\Delta\beta_1$ from the common funnel shape that is observed in fast collisions between optical beams or optical pulses in the presence of weak nonlinear dissipation. Indeed, previous works on fast collisions between time-independent beams in spatial dimension 2 [28], and between temporal optical pulses in spatial dimension 1 [22, 25, 56] in linear optical media with weak nonlinear loss showed that the graph of $\Delta A_1^{(c)}$ vs $\Delta\beta_1$ has a funnel shape and does not possess any local extrema. Similar results were obtained in Refs. [35–38] for fast collisions between optical solitons in the presence of weak nonlinear dissipation. Intuitively, the existence of the two local minima in Fig. 12 is a result of a competition between two effects. On one hand, the factor $1/|\Delta\beta_1|$ in the first line of Eq. (45), which is associated with the collision length Δz_c , leads to a decrease in the value of $\Delta A_1^{(c)}$ with increasing value

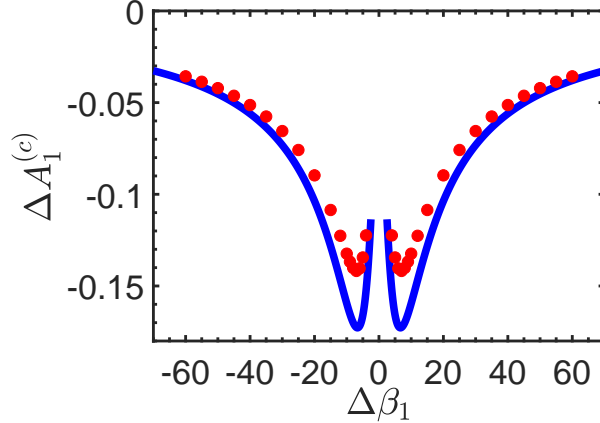


FIG. 12: (Color online) The collision-induced amplitude shift of pulsed-beam 1 $\Delta A_1^{(c)}$ vs the first-order dispersion coefficient $\Delta\beta_1$ in fast two-beam collisions with $\epsilon_3 = 0.25$ (collision setup 2). The red circles represent the result obtained by numerical simulations with Eq. (5). The solid blue curve corresponds to the perturbation theory prediction of Eq. (45).

of $|\Delta\beta_1|$. On the other hand, the dependence of the collision distance z_c on $\Delta\beta_1$ in the expressions appearing in the second and third lines of Eq. (45), which are associated with spatial beam spreading, leads to an increase in the value of $\Delta A_1^{(c)}$ with increasing value of $|\Delta\beta_1|$. The comparison between $\Delta A_1^{(c)(num)}$ and the prediction of Eq. (45) shows that this delicate competition effect is also correctly captured by our perturbation approach.

V. CONCLUSIONS

We studied fast collisions between two pulsed optical beams in a linear bulk optical medium with weak cubic loss, where the cubic loss is due to nondegenerate two-photon absorption. The collisions are induced by the difference between the first-order dispersion coefficients for the two pulsed-beams. These collisions are easier to realize than the collisions between the time-independent beams that were studied in Ref. [28]. Indeed, the latter collisions are induced by beam-steering, and therefore, their realization requires the application of special techniques to control the beam-steering. We introduced a perturbation approach for calculating the effects of a single fast two-beam collision. The approach is based on the existence of two small parameters in the problem: the cubic loss coefficient ϵ_3 and the reciprocal of the difference between the first-order dispersion coefficients $1/\Delta\beta_1$. We used

the perturbation approach to obtain general formulas for the collision-induced changes in the pulsed-beam's shape and amplitude. Moreover, we used the approach to design and characterize collision setups that lead to strong localized and nonlocalized intensity reduction effects. More specifically, the design of these setups was based on the simple form of the expression for the relative intensity reduction factor in the collision interval, which was obtained by our perturbation approach. The values of the predicted collision-induced changes in the pulsed-beam's shape were larger by one to two orders of magnitude compared with the values obtained in fast collisions between time-independent beams in Ref. [28] and in fast collisions between optical solitons in spatial dimension 1 in Ref. [39]. The predictions of our perturbation theory were in good agreement with the results of numerical simulations with the perturbed linear propagation model for both localized and nonlocalized collision setups, despite the relatively strong collisional effects.

To gain further insight into the effects of cubic loss on fast two-beam collisions, we studied the dependence of the final value of the intensity reduction factor on the z axis [$\Delta I_1^{(r)}(0, 0, z_f)$] and of the collision-induced amplitude shift ($\Delta A_1^{(c)}$) on $\Delta\beta_1$. We found that for both localized and nonlocalized collision setups, the values of $\Delta I_1^{(r)}(0, 0, z_f)$ were larger by two orders of magnitude compared with the values obtained in Ref. [28] for fast collisions between time-independent beams. The predictions of the perturbation theory were in good agreement with the numerical simulations results over the entire $\Delta\beta_1$ intervals that were considered. Moreover, since the agreement between theory and simulations improved with increasing value of $|\Delta\beta_1|$, we concluded that the significant intensity reduction effects were not limited to intermediate $|\Delta\beta_1|$ values, but also existed for large $|\Delta\beta_1|$ values.

The $\Delta\beta_1$ dependence of the collision-induced amplitude shift that was found for the nonlocalized collision setups was different from the one found for the localized setups in both theory and simulations in two important aspects. First, the values of $\Delta A_1^{(c)}$ in the nonlocalized setups were larger by one to two orders of magnitude compared with the values obtained in the localized setups. This difference was explained by noting that $\Delta A_1^{(c)}$ is a measure for global intensity changes, and that as a result, the strong but localized intensity reduction in the localized setups leads only to relatively small amplitude shifts. Second, and more importantly, the graph of $\Delta A_1^{(c)}$ vs $\Delta\beta_1$ that was obtained for the nonlocalized setups contained two local minima at intermediate values of $\Delta\beta_1$. To our knowledge, this finding represents the first observation of a deviation of the graph of $\Delta A_1^{(c)}$ vs $\Delta\beta_1$ from the common

funnel shape that is obtained in fast collisions between temporal pulses or time-independent beams in linear optical media [22, 25, 28, 56], and in fast collisions between optical solitons [35–38]. The existence of the local minima in the graph of $\Delta A_1^{(c)}$ vs $\Delta\beta_1$ was correctly captured by our perturbation theory. It was explained as a result of a competition between two effects that depend on $\Delta\beta_1$ and that affect the magnitude of $\Delta A_1^{(c)}$ in opposite manners.

In summary, we presented the first study of fast collisions between optical pulses (or optical beams) in the presence of weak nonlinear loss, in which the observed collision-induced effects are strong. We also characterized for the first time the differences between localized and nonlocalized effects in these collisions. Our perturbation approach played an important role in the design of the collision setups, and in the characterization and analysis of the strong collisional effects. In this manner, our work significantly extended the results of previous studies on fast collisions between optical pulses or time-independent beams in linear media with weak nonlinear loss [22, 25, 28, 56], and on fast collisions between optical solitons in the presence of weak nonlinear loss [35–39]. Indeed, all these previous works on the subject were limited to weak collision-induced effects, and did not characterize the differences between localized and nonlocalized effects. In view of the strong collisional effects that we observed and the fact that our perturbative calculation is based on a number of simplifying assumptions, whose validity conditions are not known, the good agreement between the perturbation theory and the simulations in the current work is quite surprising. The relatively strong intensity reduction effects can be very useful for spatial reshaping of pulsed optical beams. Additionally, our results can be useful for WDM (multisequence) optical communication systems due to the importance of fast collisions between optical pulses and optical beams in these systems.

Appendix A: Derivation of Eq. (43)

In this Appendix, we derive Eq. (43) for the inverse Fourier transforms of $\hat{g}_{12}^{(x)}(k_1, z_c) \exp[-id_{21}k_1^2(z - z_c)]$ and $\hat{g}_{12}^{(y)}(k_2, z_c) \exp[-id_{21}k_2^2(z - z_c)]$ in the case where the initial condition is given by Eq. (39). The derivations of the expressions for the two inverse Fourier transforms are very similar. In fact, we can derive the two expressions at the same time and express the end results in a single formula [Eq. (43)]. For this purpose, we introduce the symbol u , which stands for the indexes 1 or 2 in k_u , and for x or y , respectively,

everywhere else in the derivations. With this notation, we only need to obtain a single expression for the inverse Fourier transform of $\hat{g}_{12}^{(u)}(k_u, z_c) \exp[-id_{21}k_u^2(z - z_c)]$.

Using the expressions for the solutions of the unperturbed linear propagation equation, we obtain:

$$g_{12}^{(u)}(u, z_c) = \frac{W_{10}^{(u)}W_{20}^{(u)2}}{(W_{10}^{(u)4} + 4d_{21}^2z_c^2)^{1/4}(W_{20}^{(u)4} + 4d_{22}^2z_c^2)^{1/2}} \times \exp \left[-\tilde{a}_2^{(u)2}(z_c)u^2 - \frac{i}{2} \arctan \left(\frac{2d_{21}z_c}{W_{10}^{(u)2}} \right) \right], \quad (\text{A1})$$

where

$$\tilde{a}_2^{(u)2}(z_c) = q_1^{(u)}(z_c) + iq_2^{(u)}(z_c), \quad (\text{A2})$$

$$q_1^{(u)}(z_c) = \frac{W_{10}^{(u)2}}{2(W_{10}^{(u)4} + 4d_{21}^2z_c^2)} + \frac{W_{20}^{(u)2}}{W_{20}^{(u)4} + 4d_{22}^2z_c^2}, \quad (\text{A3})$$

and

$$q_2^{(u)}(z_c) = \frac{-d_{21}z_c}{W_{10}^{(u)4} + 4d_{21}^2z_c^2}. \quad (\text{A4})$$

The Fourier transform of $g_{12}^{(u)}(u, z_c)$ is

$$\hat{g}_{12}^{(u)}(k_u, z_c) = \frac{W_{10}^{(u)}W_{20}^{(u)2}(W_{10}^{(u)4} + 4d_{21}^2z_c^2)^{1/4}}{\tilde{a}_3^{(u)}(z_c)} \times \exp \left[-\frac{k_u^2}{4\tilde{a}_2^{(u)2}(z_c)} - \frac{i}{2} \arctan \left(\frac{2d_{21}z_c}{W_{10}^{(u)2}} \right) \right], \quad (\text{A5})$$

where

$$\tilde{a}_3^{(u)}(z_c) = \left[2(W_{10}^{(u)4} + 4d_{21}^2z_c^2)(W_{20}^{(u)4} + 4d_{22}^2z_c^2) \right]^{1/2} \tilde{a}_2^{(u)}(z_c). \quad (\text{A6})$$

Using Eqs. (A2)-(A6), we find that the inverse Fourier transform of $\hat{g}_{12}^{(u)}(k_u, z_c) \exp[-id_{21}k_u^2(z - z_c)]$ is given by:

$$\begin{aligned} & \mathcal{F}^{-1} \left(\hat{g}_{12}^{(u)}(k_u, z_c) \exp[-id_{21}k_u^2(z - z_c)] \right) = \\ & = \frac{W_{10}^{(u)}W_{20}^{(u)2} \exp \left[-q_1^{(u)}(z_c)u^2/R_1^{(u)4}(z, z_c) + i\chi_1^{(u)}(u, z) \right]}{(W_{10}^{(u)4} + 4d_{21}^2z_c^2)^{1/4}(W_{20}^{(u)4} + 4d_{22}^2z_c^2)^{1/2}R_1^{(u)}(z, z_c)}, \end{aligned} \quad (\text{A7})$$

where

$$R_1^{(u)}(z, z_c) = \left\{ 1 - 8d_{21}q_2^{(u)}(z_c)(z - z_c) + 16d_{21}^2 \left[q_1^{(u)2}(z_c) + q_2^{(u)2}(z_c) \right] (z - z_c)^2 \right\}^{1/4}, \quad (\text{A8})$$

and

$$\begin{aligned} \chi_1^{(u)}(u, z) = & -\frac{1}{2} \arctan \left(\frac{2d_{21}z_c}{W_{10}^{(u)2}} \right) - \frac{1}{2} \arctan \left[\frac{4d_{21}q_1^{(u)}(z_c)(z - z_c)}{1 - 4d_{21}q_2^{(u)}(z_c)(z - z_c)} \right] \\ & - \left[q_2^{(u)}(z_c) - 4d_{21} \left(q_1^{(u)2}(z_c) + q_2^{(u)2}(z_c) \right) (z - z_c) \right] \frac{u^2}{R_1^{(u)4}(z, z_c)}. \end{aligned} \quad (\text{A9})$$

Equation (A7) is Eq. (43) of subsection III A.

-
- [1] G.P. Agrawal, *Applications of Nonlinear Fiber Optics* (Academic, San Diego, CA, 2020).
 - [2] F. Forghieri, R.W. Tkach, and A.R. Chraplyvy, in *Optical Fiber Telecommunications III*, I.P. Kaminow and T.L. Koch, eds., (Academic, San Diego, CA, 1997), Chapter 8.
 - [3] L.F. Mollenauer and J.P. Gordon, *Solitons in Optical Fibers: Fundamentals and Applications* (Academic, San Diego, CA, 2006).
 - [4] R.-J. Essiambre, G. Kramer, P.J. Winzer, G.J. Foschini, and B. Goebel, *J. Lightwave Technol.* **28**, 662 (2010).
 - [5] E. Iannone, F. Matera, A. Mecozzi, and M. Settembre, *Nonlinear Optical Communication Networks* (Wiley, New York, 1998).
 - [6] S. Laroche, V. Mizrahi, and G. Stegeman, *Electron. Lett.* **26**, 1459 (1990).
 - [7] N.G.R. Broderick, D. Taverner, D.J. Richardson, M. Isben, and R.I. Laming, *Opt. Lett.* **22**, 1837 (1997).
 - [8] H.A. Haus and W.P. Huang, *Proc. IEEE* **79**, 1505 (1991).
 - [9] W.P. Huang, *J. Opt. Soc. Am. A* **11**, 963 (1994).
 - [10] R.A. Betts, J.W. Lear, N.T. Dang, R.D. Shaw, and P.S. Atherton, *IEEE Photon. Technol. Lett.* **4**, 1290 (1992).
 - [11] K. Mori, T. Morioka, and M. Saruwatari, *Opt. Lett.* **20**, 1424 (1995).
 - [12] G.P. Agrawal, *Nonlinear Fiber Optics* (Academic, San Diego, CA, 2019).
 - [13] J.D. Moores, K. Bergman, H.A. Haus, E.P. Ippen, *Opt. Lett.* **16**, 594 (1991).
 - [14] J.E. Rothenberg, *Opt. Lett.* **18**, 796 (1993).
 - [15] G.P. Agrawal, P.L. Baldeck, and R.R. Alfano, *Opt. Lett.* **14**, 137 (1989).
 - [16] J.E. Rothenberg, *Opt. Lett.* **15**, 495 (1990).
 - [17] K. Stiegitz, *Phys. Rev. E* **63**, 016608 (2000).

- [18] R.A. Negres, J.M. Hales, A. Kobayakov, D.J. Hagan, and E.W. Van Stryland, *IEEE J. Quantum Electron.* **38**, 1205 (2002).
- [19] C.M. Cirloganu, L.A. Padilha, D.A. Fishman, S. Webster, D.J. Hagan, and E.W. Van Stryland, *Opt. Express* **19**, 22951 (2011).
- [20] In particular, the collision length is much smaller than the dispersion length and/or the diffraction length.
- [21] G.P. Agrawal, *Fiber-Optic Communication Systems* (Wiley, New York, 1997).
- [22] A. Peleg, Q.M. Nguyen, and T.T. Huynh, *Eur. Phys. J. D* **71**, 315 (2017).
- [23] L.F. Mollenauer, A. Grant, X. Liu, X. Wei, C. Xie, and I. Kang, *Opt. Lett.* **28**, 2043 (2003).
- [24] M. Nakazawa, *IEEE J. Sel. Top. Quant. Electron.* **6**, 1332 (2000).
- [25] Q.M. Nguyen, T.T. Huynh, and A. Peleg, *Indian J. Phys.* **96**, 453 (2022).
- [26] In this paper, we adopt the common terminology in nonlinear waveguide optics and refer to solitons of the cubic nonlinear Schrödinger equation as optical solitons. This terminology is adopted since the cubic nonlinear Schrödinger equation describes propagation of pulses of light in a wide variety of nonlinear optical waveguides [12].
- [27] A. Peleg, M. Chertkov, and I. Gabitov, *Phys. Rev. E* **68**, 026605 (2003).
- [28] A. Peleg, T.T. Huynh, and Q.M. Nguyen, *J. Eng. Math.* **132**, 23 (2022).
- [29] P.F. McManamon, P.J. Bos, M.J. Escuti, J. Heikenfeld, S. Serati, H. Xie, E.A. Watson, *Proc. IEEE* **97**, 1078 (2009).
- [30] P. Brandl, S. Schidl, A. Polzer, W. Gaberl, H. Zimmermann, *IEEE Photon. Technol. Lett.* **25**, 1428 (2013).
- [31] C.W. Oh, Z. Cao, E. Tangdionga, T. Koonen, *Opt. Express* **24**, 19211 (2016).
- [32] A.E. Siegman, *Lasers* (University Science Books, Mill Valley, CA, 1986).
- [33] H. Kogelnik and T. Li, *Appl. Opt.* **5**, 1550 (1966).
- [34] Here we define the spatial dimension of the problem as the number of coordinates on which the electric field depends for a given distance. Therefore, in Refs. [22, 25], the spatial dimension was 1, in Refs. [28] it was 2, and in the current paper it is 3.
- [35] A. Peleg, Q.M. Nguyen, and Y. Chung, *Phys. Rev. A* **82**, 053830 (2010).
- [36] A. Peleg and Y. Chung, *Phys. Rev. A* **85**, 063828 (2012).
- [37] Q.M. Nguyen and T.T. Huynh, *Nonlinear Dyn.* **104**, 4339 (2021).
- [38] Q.M. Nguyen and T.T. Huynh, *Wave Random Complex*, "Impact of two-photon absorption

- on two-dimensional solitons in silicon waveguides with a nonstationary potential”, in press (DOI: 10.1080/17455030.2021.2008546).
- [39] A. Peleg and D. Chakraborty, *Physica D* **406**, 132397 (2020).
- [40] Q. Lin, O.J. Painter, and G.P. Agrawal, *Opt. Express* **15**, 16604 (2007).
- [41] R. Dekker, N. Usechak, M. Först, and A. Driessen, *J. Phys. D* **40**, R249 (2007).
- [42] M. Borghi, C. Castellan, S. Signorini, A. Trenti, and L. Pavesi, *J. Opt.* **19**, 093002 (2017).
- [43] R.W. Boyd, *Nonlinear Optics* (Academic, San Diego, CA, 2008).
- [44] J.E. Ehrlich, X.L. Wu, I.-Y.S. Lee, Z.-Y. Hu, H. Röckel, S.R. Marder, J.W. Perry, *Opt. Lett.* **22**, 1843 (1997).
- [45] T.K. Liang, L.R. Nunes, T. Sakamoto, K. Sasagawa, T. Kawanishi, M. Tsuchiya, G.R.A. Priem, D. Van Thourhout, P. Dumon, R. Baets, H.K. Tsang, *Opt. Express* **13**, 7298 (2005).
- [46] R. Jones, H. Rong, A. Liu, A.W. Fang, M.J. Paniccia, D. Hak, O. Cohen, *Opt. Express* **13**, 519 (2005).
- [47] A. Liu, H. Rong, M.J. Paniccia, O. Cohen, D. Hak, *Opt. Express* **12**, 4261 (2004).
- [48] Y.S. Kivshar and B.A. Malomed, *Rev. Mod. Phys.* **61**, 763 (1989).
- [49] V. Mizrahi, K.W. DeLong, G.I. Stegeman, M.A. Saifi, and M.J. Andrejco, *Opt. Lett.* **14**, 1140 (1989).
- [50] A.B. Aceves and J.V. Moloney, *Opt. Lett.* **17**, 1488 (1992).
- [51] E.N. Tsoy, C.M. de Sterke, and F.Kh. Abdullaev, *J. Opt. Soc. Am. B* **18**, 1144 (2001).
- [52] Y. Okawachi, O. Kuzucu, M.A. Foster, R. Salem, A.C. Turner-Foster, A. Biberman, N. Ophir, K. Bergman, M. Lipson, and A.L. Gaeta, *IEEE Photon. Technol. Lett.* **24**, 185 (2012).
- [53] A. Peleg, D. Chakraborty, *Phys. Rev. A* **98**, 013853 (2018).
- [54] M.A. Foster, A.C. Turner, M. Lipson, and A.L. Gaeta, *Opt. Express* **16**, 1300 (2008).
- [55] C. Rauscher and R. Laenen, *J. Appl. Phys.* **81**, 2818 (1997).
- [56] Q.M. Nguyen, *Int. J. Nonlinear Sci. Numer. Simulat.* **23**, 335 (2022).
- [57] A. Ishimaru, *Electromagnetic Wave Propagation, Radiation, and Scattering* (Wiley, Hoboken, NJ, 2017).
- [58] See also Ref. [28], where a similar nondimensionalization process was carried out for time-independent beams.
- [59] J. Yang, *Nonlinear Waves in Integrable and Nonintegrable Systems* (SIAM, Philadelphia, 2010).

- [60] I.H. Malitson, J. Opt. Soc. Am. **55**, 1205 (1965).
- [61] C.Z. Tan, J. Non-Cryst. Solids **223**, 158 (1998).
- [62] Notice that with this choice, $\beta_{22} = 1.0060$, $d_{21} = 0.06$, and $d_{22} = 0.06009$. However, since the values of the collision-induced changes in the shapes and amplitudes of the pulsed-beams are not sensitive to the exact values of these parameters, we use for simplicity $\beta_{22} = 1.0$ and $d_{22} = 0.06$ in the numerical simulations in setup 1.
- [63] We choose to present the pulsed-beam shapes using cross-sections, since this enables a clearer presentation of the dynamics of the main bodies of the pulsed-beams compared with conventional contour plots. Indeed, in the latter plots, the main bodies of the pulsed-beams are typically obscured by the outer parts (i.e., by the pulsed-beams tails). The three cross-sections are chosen as the planes, $x = 0$, $t = 0$, and $t = t_2(z)$, where $t_2(z)$ is the time coordinate of the center of pulsed-beam 2 at distance z .
- [64] The value of z_i is determined by: $z_i = z_c + r(z_f - z_c)$, where $r = 1/5$, as an example. Thus, z_i is an intermediate distance that is larger than z_c , at which the collision is not yet completed.
- [65] Since the fractional intensity reduction factor obtained in the simulations $\Delta I_1^{(r)(num)}(t, x, y, z)$ shows moderate dependence on t , we calculate $\Delta I_1^{(r)(num)}(x, y, z)$ by using the value of $\Delta I_1^{(r)(num)}(0, x, y, z)$. We emphasize that a similar result is obtained by averaging $\Delta I_1^{(r)(num)}(t, x, y, z)$ over some time interval centered about $t = 0$, e.g., $[-2, 2]$. Similar methods were used to obtain $\Delta I_1^{(r)(num)}(y, z)$ in fast collisions between time-independent beams in Ref. [28].
- [66] Notice that with this choice, $\beta_{22} = 1.0060$, $d_{21} = 1.0$, and $d_{22} = 1.0014$. However, since the values of the collision-induced changes in the pulsed-beams' shapes and amplitudes are not sensitive to the exact values of these parameters, we use for simplicity $\beta_{22} = 1.0$ and $d_{22} = 1.0$ in the numerical simulations in setup 2.